



UNIVERSITY OF LEEDS

This is a repository copy of *Ammonium ocean following the end-Permian mass extinction*.

White Rose Research Online URL for this paper:

<http://eprints.whiterose.ac.uk/147828/>

Version: Accepted Version

---

**Article:**

Sun, YD, Zulla, MJ, Joachimski, MM et al. (4 more authors) (2019) Ammonium ocean following the end-Permian mass extinction. *Earth and Planetary Science Letters*, 518. pp. 211-222. ISSN 0012-821X

<https://doi.org/10.1016/j.epsl.2019.04.036>

---

© 2019 Elsevier B.V. Licensed under the Creative Commons Attribution-NonCommercial-NoDerivatives 4.0 International License (<http://creativecommons.org/licenses/by-nc-nd/4.0/>).

**Reuse**

This article is distributed under the terms of the Creative Commons Attribution-NonCommercial-NoDerivatives (CC BY-NC-ND) licence. This licence only allows you to download this work and share it with others as long as you credit the authors, but you can't change the article in any way or use it commercially. More information and the full terms of the licence here: <https://creativecommons.org/licenses/>

**Takedown**

If you consider content in White Rose Research Online to be in breach of UK law, please notify us by emailing [eprints@whiterose.ac.uk](mailto:eprints@whiterose.ac.uk) including the URL of the record and the reason for the withdrawal request.



[eprints@whiterose.ac.uk](mailto:eprints@whiterose.ac.uk)  
<https://eprints.whiterose.ac.uk/>



14 **Abstract:** The aftermath of end-Permian mass extinction was marked by a ~5 million year  
15 interval of poorly-understood, extreme environments that likely hindered biotic recovery.  
16 Contemporary nitrogen isotope variations are considered, using a new conceptual model,  
17 to support a scenario that shows intensive nitrate-removal processes gradually depleted  
18 the global oceanic nitrate inventory during long-lasting oceanic anoxia. Enhanced nitrogen  
19 fixation shifted the oceanic nitrogenous nutrient (nutrient-N) inventory to an ammonium-  
20 dominated state. Ammonium is toxic to animals and higher plants but fertilizes algae and  
21 bacteria. This change in ocean chemistry could account for the intense and unexplained  
22 losses of nektonic taxa and the proliferation of microbial blooms in the Early Triassic. The  
23 transition from a nitrate ocean to an ammonium ocean was accompanied by a decrease in  
24 respiration efficiency of organisms and a shrinking oceanic nutrient-N inventory,  
25 ultimately leading to generally low productivity in the Early Triassic oceans. These  
26 unappreciated nutrient changes during episodes of prolonged ocean anoxia may be the key  
27 life-limiting factor at such times.

28

29 Key words: ocean anoxic event, nitrogen cycle, Early Triassic, ammonium ocean

30

## 31 **1. Introduction**

32           Following the most devastating extinction of the Phanerozoic, the Early Triassic  
33 (~253-247 Ma) interval is considered to have been an extreme hothouse world (Kidder  
34 and Worsley, 2010; Winguth et al., 2015) with equatorial sea-surface temperatures (SSTs)  
35 consistently higher than 32 °C (Sun et al., 2012). Such temperature extremes reduce the  
36 solubility of all gases in the ocean, decrease photosynthetic efficiency in terrestrial plants  
37 and phytoplankton and increase metabolic energy demands (approximately double the  
38 cost for every 10 °C rise according to the  $Q_{10}$  temperature coefficient), and can lead to  
39 intense oceanic anoxia, low biodiversity, and animals with small body sizes (Wignall and  
40 Twitchett, 2002; Twitchett, 2007; Bottjer et al., 2008). The peak of the hothouse occurred  
41 during the Smithian-Spathian (S-S) transition, ~2 million years after the end-Permian mass  
42 extinction, when equatorial SSTs reached ~40 °C (Sun et al., 2012) during a major ~6-8 ‰  
43 negative carbon isotope excursion (Payne et al., 2004; Sun et al., 2015). Many nektonic taxa  
44 that were well adapted to the harsh post-extinction environments finally succumbed at the  
45 S-S transition, suffering even greater proportional losses than at the end of the Permian  
46 (Stanley, 2009).

47           The warm climate and concomitant increased weathering and continental runoff in  
48 the Early Triassic enhanced nutrient delivery to the oceans (Algeo et al., 2011),  
49 theoretically elevating primary productivity and amplifying oxygen deficiency in the water  
50 column (Kump et al., 2005), ultimately producing euxinia with noxious H<sub>2</sub>S. Such  
51 conditions exist today as localized “dead zones” like those found in the Gulf of Mexico  
52 (Rabalais et al., 2002), and they are an oft-cited mechanism for the end-Permian marine  
53 extinction and the delayed Early Triassic recovery (Kump et al., 2005; Algeo et al., 2011).

54 All versions of the death-by-anoxia (euxinia) scenario assume that phosphorus (P) was the  
55 key bio-essential element that controlled productivity levels (Meyer et al., 2008).  
56 Cyanobacterial biomarker spikes and the development of microbialites during and in the  
57 immediate aftermath of the end-Permian crisis (Pruss et al., 2006; Xie et al., 2010)  
58 potentially reflect this high productivity scenario.

59 In addition to P, the other productivity-limiting nutrient in the ocean is N. Unlike P,  
60 nutrient-N availability is not a function of terrestrial input since the oceanic N cycle is  
61 largely internal and biologically-driven (Sigman et al., 2009) (Fig. 1). Under anoxic  
62 conditions denitrification is enhanced and removes nitrate (including nitrite) as N<sub>2</sub> while P  
63 is released from sediments (Van Cappellen and Ingall, 1994). This process, if widespread  
64 and maintained for a prolonged time, generates a nitrate-poor but P-rich ocean (Grasby et  
65 al., 2012; Grasby et al., 2016). The Early Triassic is known for global absence of  
66 phosphorites and other P-rich sedimentary rocks, suggesting intensive P-recycling into  
67 seawater at this time. Although P can be additionally and partially scavenged by Fe  
68 minerals (Feely et al., 1991), Fe shuttles in the Early Triassic oceans were dominated by  
69 pyrite burial, and quantitatively not comparable to banded iron formation deposition in the  
70 Archean and Paleoproterozoic oceans. Thus, P scavenged by Fe minerals is unlikely to have  
71 balanced the excess P input by weathering. Nitrogen could have become the bio-limiting  
72 nutrient in the euphotic zone since marine phytoplankton requires 14-16 times more N  
73 than P (i.e., the Redfield Ratio). The high SSTs of the Early Triassic (Sun et al., 2012) likely  
74 deepened the thermocline, lowered the pole-to-equator temperature gradient and  
75 weakened ocean circulation (Winguth et al., 2015). Under such circumstances, PO<sub>4</sub><sup>3-</sup> and

76  $\text{NO}_3^-$  were probably trapped beneath density barriers, inhibiting nutrient supply to the  
77 euphotic zone (Fig. 2C; Grasby et al., 2016; Penn et al., 2018).

78 To understand the interplay of stratification intensity and the availability of  
79 different nutrients in the Early Triassic oceans, we investigated nitrogen isotope ( $\delta^{15}\text{N}$ )  
80 trends and trace metal concentrations during the Late Permian to Early Triassic in palaeo-  
81 equatorial Tethys (Xiakou and Jiarong sections, South China) and the Boreal Ocean  
82 (Vindodden section, Spitsbergen) (Fig. 2). The results, combined with our new conceptual  
83 model (Fig. 1), suggest the establishment of an “Ammonium Ocean” had severe  
84 consequences for the marine biosphere in the Early Triassic.

85

## 86 **2. Settings**

87 The South China Block was situated at an equatorial position in the eastern Tethys  
88 Ocean in the Early Triassic (Fig. 2A). Palaeogeographically, the study section at Xiakou was  
89 situated on the northern margin of the central Yangtze Platform. The study section at  
90 Jiarong was situated in the centre of the Nanpanjiang Basin, which was a V-shaped, deep  
91 water epicontinental basin that opened south-eastward to the Panthalassa Ocean  
92 (Lehrmann et al., 2003).

93 The Xiakou section (GPS:  $31^\circ 6'55.82''\text{N}$ ,  $110^\circ 48'15.87''\text{E}$ ) is located in Xingshan  
94 County, ~400 km NW of Wuhan. The continuous sequence, from late Changhsingian to  
95 Spathian, crops out alongside a local road. The late Changhsingian strata are characterized  
96 by dark grey to black, marly carbonate and marls. The lithology is replaced upsection by  
97 thinly bedded grey carbonate and shales of the Daye Formation.

98           The Jiarong section (GPS: 25°55'17"N, 106°33'50"E) is located in Huishui County,  
99   ~85 km south of Guiyang City in the Guizhou Province. The Smithian-Spathian succession is  
100 composed of a middle-late Smithian carbonate unit, a latest Smithian black shale unit and  
101 an early Spathian reddish carbonate unit, representing a transition from a basinal setting to  
102 a shallower water environment across the S-S boundary interval (Chen et al., 2015; Sun et  
103 al., 2015). Sediments in the upper part of the Carbonate Unit and the Black Shale Unit are  
104 finely laminated and lack bioturbation. Fossils are generally rare, except for conodonts.  
105 Small ammonoids and scaphopods occur in the Spathian Griotte Unit (Sun et al., 2015).

106           During the Permo-Triassic the Svalbard Archipelago was situated on the  
107 epicontinental shelf of the northern passive margin of Pangaea adjacent to the Boreal  
108 Ocean in high temperate latitudes (~ 55 to 60 °N) (Hounslow et al., 2008). The S-S strata of  
109 central Spitsbergen belong to the Vikinghøgda Formation, and are best documented from  
110 the Vindodden section (Mørk et al., 1999; Wignall et al., 2016).

111           The Vindodden section (GPS: 78°19'39"N, 16°30'19"E) lies in the lower slopes of  
112 Botneheia Mountain, south of Sassenfjorden, a north-eastern arm of Isfjorden. The S-S  
113 sequence consists mainly of a lower unit of dark clay/siltstone unit of Smithian age and an  
114 upper siltstone-sandstone unit of Spathian age. The transition from the Smithian to the  
115 Spathian is marked by a laminated thin dolostone ledge of earliest Spathian age. The  
116 phosphatic black clay/shales atop the Vikinghøgda Formation characterise the Middle  
117 Triassic Botneheia Formation (Wignall et al., 2016). Fossils are rare in the study section,  
118 except for a few *Posidonia* bivalves, *Planolites* trace fossils and ammonoids. Though very  
119 low in abundance, conodonts occur throughout the section, providing biostratigraphic  
120 constraints.

121

### 122 **3. Conceptual Model**

123 Our conceptual model for the oceanic nitrogen cycle consists of four end-members.  
124 They are  $N_2$ , the  $NH_4^+/NH_3$  pair, the  $NO_2^-/NO_3^-$  pair and organic-bonded nitrogen. Amongst  
125 these,  $NH_4^+/NH_3$  and  $NO_2^-/NO_3^-$  are the main forms of dissolved inorganic nutrient-N in the  
126 ocean. The four end-members are linked by eight known reactions in the nitrogen cycle  
127 (Fig. 1). These reactions are further subdivided into aerobic reactions (e.g., nitrification),  
128 anaerobic reactions (e.g., denitrification) and non-redox sensitive reactions (e.g., nitrogen  
129 fixation). This subdivision leads to three simplified sub-models for oceanic nitrogen cycle  
130 in fully oxic (Fig. 1 model A), fully anoxic (Fig. 1 model B) and fully euxinic conditions (Fig.  
131 1 model C). In modern ocean settings, the oceanic nitrogen cycle is dominated by processes  
132 summarized in the model A, while model B describes the nitrogen cycle in the oxygen  
133 minimum zone (OMZ). In warm, stratified and oxygen-depleted Early Triassic oceans, the  
134 models B and C describes the main oceanic nitrogen cycle with the model A only applicable  
135 to the thin, oxygenated surface layer. Though nitrification is an aerobic reaction, it can  
136 occur at very low oxygen concentrations at a lower rate (Bristow et al., 2016). In such  
137 cases, the dissolved nutrient-N inventory is in a subtle balance between nitrate net  
138 production and net consumption, depending on the intensity of ocean anoxia. For example,  
139 at the Black Sea thermocline, anaerobic ammonium oxidation (anammox) bacteria  
140 outcompete aerobic nitrifying bacteria for nitrite (Lam et al., 2007), leading to nitrate and  
141 nitrite net consumption.

142 Nitrate production by nitrification is mainly carried out by ammonia-oxidizing  
143 bacteria (AOB) and ammonia-oxidizing archaea (AOA). This process is generally considered

144 to be light-sensitive for two reasons: 1) some AOB show photoinhibition (e.g., Guerrero and  
145 Jones, 1996), and 2) AOA, though more abundant than AOB in the euphotic zone and not  
146 light-inhibited *per se*, are often outcompeted by phytoplankton for  $\text{NH}_4^+$ . The rate of  
147 nitrification of AOA is lower in the euphotic zone during the day and in the summer due to  
148 limited  $\text{NH}_4^+$  supply while the highest rate occurs at night and in the winter when  
149 competition with phytoplankton is lowest (Smith et al., 2014). Because the euphotic zone is  
150 only a thin layer of water column, the overall rates and efficiency of nitrification in the  
151 ocean depend critically on general redox conditions below the euphotic zone (e.g., Quan  
152 and Falkowski, 2009).

153 Denitrification has a high energy yield (Table 1) and the resupply of nitrate by  
154 nitrification is greatly inhibited in anoxic conditions. Thus, quantitatively nitrate must be in  
155 net consumption in intensive anoxic and euxinic oceans because nitrate produced by  
156 nitrification in the thin, oxygenated surface water column cannot compensate for the  
157 nitrate consumed by denitrification and anammox in anoxic and much thicker deeper  
158 water columns (Fig. 2C). Note that anaerobic ammonium oxidation by manganese oxides  
159 occurs in sediments rather than the water column (e.g., Hulth et al., 1999) and is excluded  
160 here.

161 We use the notion “ammonium ocean” to describe an oceanic state in which  $\text{NO}_2^-$   
162 and  $\text{NO}_3^-$  are largely depleted while  $\text{NH}_4^+$  is the main form of dissolved nutrient-N. Note  
163 that dominance is not necessarily equal to high concentrations. Thus the term “ammonium  
164 ocean” does not necessarily imply *globally* high  $\text{NH}_4^+$  concentrations in the ocean (see 5.3  
165 for further discussion on the heterogeneity of Early Triassic oceans).

166

#### 167 4. Methods (isotope and C/N ratio analyses)

168 For measurements of  $\delta^{13}\text{C}_{\text{org}}$ ,  $\delta^{15}\text{N}$ , and  $\text{C}/\text{N}_{\text{atomic}}$  ratios, weathered surfaces were cut  
169 off the samples. The trimmed samples were washed with distilled water, dried with  
170 compressed air and then milled to fine powder. On average  $\sim 3$  to  $\sim 5$  g powders were  
171 immediately treated with  $\sim 150$  ml 10 % HCl on a hotplate at  $\sim 60$  °C to dissolve any  
172 carbonate. The samples were stirred while slowly adding acid. The decarbonatization  
173 process was generally completed after 48 hours with the complete removal of dolomite and  
174 siderite phases. If not, acid was refreshed and the samples were treated further for 24-48  
175 hours. Insoluble residues were washed repeatedly with deionized water until  $\text{pH} \approx 6$ , dried  
176 in an oven at 60 °C, homogenized using a mortar and stored in small glass containers.

177 The  $\delta^{13}\text{C}_{\text{org}}$  and bulk rock  $\delta^{15}\text{N}$  analyses were performed with a Flash EA 2000  
178 elemental analyser connected online to ThermoFinnigan Delta V Plus mass spectrometer.  
179 All isotope values are reported in the conventional  $\delta$ -notation in per mille (‰) relative to  
180 atmospheric air for  $\delta^{15}\text{N}$  and to V-PDB for  $\delta^{13}\text{C}_{\text{org}}$ . Reproducibility of measurements was  
181 monitored by replicate analyses of laboratory standards (synthetic urea) calibrated to  
182 international standards USGS 40 ( $\delta^{13}\text{C} = -26.39$  ‰;  $\delta^{15}\text{N} = -4.52$  ‰) and USGS 41 ( $\delta^{13}\text{C} =$   
183  $37.63$  ‰;  $\delta^{15}\text{N} = 47.57$  ‰). The reproducibility was  $\pm 0.08$  ‰ ( $2\sigma$ ) for  $\delta^{13}\text{C}_{\text{org}}$ ,  $\pm 0.07$  ‰  
184 ( $2\sigma$ ) for total organic carbon (TOC),  $\pm 0.14$  ‰ ( $2\sigma$ ) for  $\delta^{15}\text{N}$  and  $\pm 0.20$  ‰ ( $2\sigma$ ) for total  
185 nitrogen (TN). The repeatability of samples for  $\delta^{15}\text{N}$  ranges from 0.05 to 0.18 ‰ ( $2\sigma$ ), with  
186 a single case of 0.42 ‰. Note that our  $\delta^{15}\text{N}$  data, as in many other studies in this interval,  
187 represent a  $\delta^{15}\text{N}_{\text{acidified}}$  (rather than  $\delta^{15}\text{N}_{\text{bulk}}$ ) record in a strict sense. The  $\text{C}/\text{N}_{\text{atomic}}$  ratio was  
188 calculated from  $(\text{TOC}/\text{atomic weight of C})/(\text{TN}/\text{atomic weight of N})$ . The TN and TOC  
189 values are positively correlated ( $r^2 = 0.42, 0.68$  and  $0.93$  for Jiarong, Vindodden and Xiakou

190 sections, respectively), suggesting organic matter was the primary source of N (Fig. 3).  
191 Other sources include clay-bound N resulting from diagenetic  $\text{NH}_4^+$  release. The occurrence  
192 of clay-bound N may homogenise, but not necessarily perturb,  $\delta^{15}\text{N}$ .

193 For  $\delta^{13}\text{C}_{\text{carb}}$  analyses, carbonate powders, preferably from micrites, were drilled on  
194 fresh-cut rock surfaces. The powders were reacted with 100 % phosphoric acid at 70 °C in  
195 a Gasbench II connected online with a ThermoFinnigan Delta V Plus mass spectrometer. All  
196 values are reported in per mille relative to V-PDB by assigning  $\delta^{13}\text{C}$  values of +1.95 ‰ to  
197 NBS19 and -47.3 ‰ to IAEA-CO9 and  $\delta^{18}\text{O}$  values of -2.20 ‰ to NBS19 and -23.2 ‰ to  
198 NBS18. Reproducibility was monitored by replicate analysis of laboratory standards  
199 calibrated to NBS 19 and NBS18, and was  $\pm 0.04$  ‰ for  $\delta^{13}\text{C}_{\text{carb}}$  and  $\pm 0.04$  ‰ for  $\delta^{18}\text{O}_{\text{carb}}$   
200 ( $2\sigma$ ;  $n = 20$ ).

201

## 202 **5. Perturbations in global carbon and nitrogen cycles in the Early Triassic**

203 The  $\delta^{13}\text{C}_{\text{carb}}$  values of the Xiakou section show an increase from 1.22 to 2.16 ‰ in  
204 the late Changhsingian. This positive trend is followed by a negative excursion of -2.8 ‰  
205 across the Permian-Triassic (P-T) boundary (at 0 m height). A second,  $\sim -2.0$  ‰ negative  
206 excursion occurs in the mid-late Griesbachian. The largest negative excursion of  $\sim -3.0$  ‰  
207 amplitude occurs in the Smithian.  $\delta^{13}\text{C}_{\text{carb}}$  values decrease from 2.04 to -1.00 ‰ and  
208 remain low in the late Smithian (Fig. 4).

209 The  $\delta^{13}\text{C}_{\text{org}}$  values of Jiarong and Vindodden sections show a similar pattern in the S-  
210 S transition, but differ in absolute values by  $\sim 1$  ‰.  $\delta^{13}\text{C}_{\text{org}}$  from Jiarong shows a positive  
211 excursion of  $\sim 5.5$  ‰ from -31.5 ‰ in the late Smithian to -26.0 ‰ in the earliest Spathian.

212 A slightly smaller positive excursion of  $\sim 4.5$  ‰ is registered at Vindodden, with values  
213 increasing from  $-32.5$  to  $-28.0$  ‰ across the S-S boundary (at 56 m height; Fig. 4).

214 The  $\delta^{13}\text{C}_{\text{carb}}$  and  $\delta^{13}\text{C}_{\text{org}}$  variations from our study sections are consistent with  
215 published  $\delta^{13}\text{C}$  records (Payne et al., 2004; Grasby et al., 2012), and are therefore  
216 considered to record the global signature. The difference in absolute  $\delta^{13}\text{C}_{\text{org}}$  values between  
217 Jiarong and Vindodden is attributed to different primary producers between the equatorial  
218 and Boreal oceans, which were likely to show different carbon isotopic fractionation during  
219 photosynthesis. The  $\delta^{13}\text{C}$  perturbations, redox and sedimentary changes support a scenario  
220 that intense oceanic anoxia in the late Smithian contributed to enhanced burials of organic  
221 carbon (i.e., black shale deposition and positive  $\delta^{13}\text{C}$  excursion) (Sun et al., 2015).

222 The  $\delta^{15}\text{N}$  values from Xiakou record a rapid increase in the late Changhsingian and  
223 reached a  $\sim 3$  ‰ peak immediately above the P-T boundary (Fig. 4). This was followed by a  
224 protracted, gradual decrease from the early Griesbachian to values of  $\sim 0.5$  ‰ in the late  
225 Smithian. At Jiarong,  $\delta^{15}\text{N}$  values match those at Xiakou and then decrease to  $\sim -1$  ‰ across  
226 the S-S boundary (at 24.3 m height); a level that sees the onset of black shale deposition. A  
227 comparable trend across the S-S transition is seen at Vindodden although the  $\delta^{15}\text{N}$  curve is  
228 offset in absolute value by  $\sim 1$  ‰ compared with the other sections (Fig. 4). The  $\text{C}/\text{N}_{\text{atomic}}$   
229 ratio (a measure of organic matter stoichiometry) generally co-varies with, but is opposite  
230 to, the observed trends in  $\delta^{15}\text{N}$ . Thus,  $\text{C}/\text{N}_{\text{atomic}}$  at Xiakou decreases sharply across the P-T  
231 boundary from  $>20$  to  $\sim 2$ , followed by a mild recovery to  $\sim 10$  in the Dienerian and  
232 oscillations around  $\sim 6$  in the Smithian.  $\text{C}/\text{N}_{\text{atomic}}$  at Jiarong increases steadily from  $\sim 10$  to  
233  $\sim 30$  towards the S-S boundary, followed by a decrease above its maxima of  $\sim 40$  in the

234 earliest Spathian. At Vindodden,  $C/N_{\text{atomic}}$  increases from  $\sim 11$  to  $\sim 20$  towards the S-S  
235 boundary (at 56 m height) before decreasing to  $\sim 15$  in the early Spathian.

236 The  $\delta^{15}\text{N}$  data show minor regional variations compared to published records, with  
237 differences occurring mainly in the Late Permian (Fig. 5). Water column denitrification  
238 occurred near the P-T boundary at Xiakou whereas in Arctic Canada and western Alberta  
239 denitrification prevailed in the late [st](#) Permian. The  $\delta^{15}\text{N}$  shifts seen in the Early Triassic at  
240 Xiakou and Jiarong are comparable to reported patterns from the Sverdrup Basin (Knies et  
241 al., 2013; Grasby et al., 2016) and the western margin of Pangaea (Schoepfer et al., 2012).  
242 Since South China, the Sverdrup Basin and western Alberta were situated in very different  
243 climatic and oceanographic settings, and yet were connected to the Panthalassa ocean, we  
244 interpret their comparable  $\delta^{15}\text{N}$  variations in the Early Triassic to reflect the global ocean  
245 signatures (Fig. 5). The divergence in  $\delta^{15}\text{N}$  between Vindodden and other regions probably  
246 reflects a minor nitrate input from a polar current to Spitsbergen as well as its slightly  
247 more restricted environment (Fig. 2A).

248

## 249 **6. Discussion**

### 250 *6.1 Influence of diagenesis on $\delta^{15}\text{N}$ and $C/N_{\text{atomic}}$ ratio*

251 Diagenesis can potentially alter both sedimentary  $\delta^{15}\text{N}$  and the  $C/N_{\text{atomic}}$  ratio. For  
252 example, degradation of amino acid during early diagenesis releases  $\text{NH}_4^+$  to pore water. If  
253 the  $\text{NH}_4^+$  is absorbed by clay minerals, then sedimentary  $\delta^{15}\text{N}$  would show minor changes  
254 compared to the original signature. Positive intercepts on the TN axis in our TN-TOC cross  
255 plot (Fig. 3) indicate the presence of excess clay-bound nitrogen in our samples. We  
256 consider our  $\delta^{15}\text{N}$  to a be [a](#) faithfully record because data measured from adjacent

257 carbonate and marl (shale) samples, although with large variations in TOC and clay  
258 content, show consistent values in  $\delta^{15}\text{N}$  (Table 2) and our sections are from different  
259 sedimentary basins and underwent different diagenetic and burial history, and yet the  $\delta^{15}\text{N}$   
260 records are largely comparable with each other and published records. Only, the onset and  
261 duration of P-T water column denitrification show regional variations (Fig. 5). On the other  
262 hand, diagenesis can significantly alter the  $\text{C}/\text{N}_{\text{atomic}}$  ratio, especially in TOC-poor, clay-rich  
263 sediments, and cause divergence from the Redfield Ratio to higher values. Diagenetic  
264 sulphate reduction, which removes C but not N, can lower  $\text{C}/\text{N}_{\text{atomic}}$  ratio.

## 265 *6.2 Intensified denitrification, low sulphate concentration and a nitrate starved ocean*

266 The oceanic N cycle is largely microbially mediated (Altabet, 2006). The onset of  
267 intense and widespread anoxia in the latest Permian saw a profound change in dominance  
268 amongst oceanic microbial communities from aerobic to anaerobic respiration. Since the  
269 energy yield from denitrification ( $\Delta G^0 = -445 \text{ kJ/mol C}$ )<sup>1</sup> is almost as efficient as that of  
270 aerobic respiration ( $\Delta G^0 = -478 \text{ kJ/mol C}$ ), nitrate is the first energy source to be consumed  
271 in anoxic environments (Table 1). Thus, the shift to microbial anaerobic respiration is  
272 manifest as the positive  $\delta^{15}\text{N}$  trend seen in the late Changhsingian at Xiakou and elsewhere  
273 (Fig. 5). This indicates widespread water column denitrification, and coincides with the  
274 onset of intensive anoxia (e.g., Grasby et al., 2012; Elrick et al., 2017).

275 Despite some regional variations,  $\delta^{15}\text{N}$  records from different settings all indicate  
276 strong denitrification occurring across the P-T boundary, followed by a dominance of

---

<sup>1</sup>  $\Delta G^0$  represents the standard Gibbs free energy of formation, a thermodynamic measure of energy absorption or yield of a reaction at the standard conditions (25 °C and 100 kPa). Positive values suggest a reaction absorbs energy while negative values suggest a reaction yield energy. The more negative the values, the more energy is yielded though the reaction.

277 | [nitrogen fixation in the Early Triassic \(Fig. 5\)](#). The  $\delta^{15}\text{N}$  values in the Early Triassic of our  
278 study sections are depleted in  $^{15}\text{N}$  compared to the average  $\delta^{15}\text{N}$  of modern oceans ( $\sim 5$   
279 ‰)(Altabet, 2007). Nitrate was likely depleted and nitrogen fixation dominated in both  
280 northern Boreal and equatorial Tethyan waters at this time. Reducing conditions amplify  
281 anaerobic reactions such as denitrification and anammox; reactions that selectively  
282 consume nitrate depleted in  $^{15}\text{N}$  ( $\epsilon = 5\text{--}30$  ‰) and produce non-nutritious  $\text{N}_2$ . As nitrate  
283 consumption continues,  $^{15}\text{N}$  becomes enriched in seawater, resulting in heavy  $\delta^{15}\text{N}$  values  
284 in sedimentary organic matter (e.g.  $\delta^{15}\text{N} > 5$  ‰). In modern oceans, intensive  
285 denitrification occurs in the oxygen minimum zone where organic matter and nitrate are  
286 both replete (Fig. 2C). In the Early Triassic anoxic oceans, denitrification and anammox  
287 probably occurred over a broad range of depths and theoretically would have generated  
288 high sedimentary  $\delta^{15}\text{N}$  values (e.g.  $\delta^{15}\text{N} = \sim 5\text{--}15$  ‰). Instead,  $\delta^{15}\text{N}$  values from both  
289 equatorial and boreal settings are in the  $-1$  to  $2$  ‰ range. This can be explained through a  
290 nitrate-starved scenario in which the isotopic fractionation effect of denitrification and  
291 anammox decreases due to very low nitrate availability (i.e., exceptionally high  
292 denitrification rate) and intense seawater stratification while nitrogen fixation is the only  
293 source of nutrient-N. Alternatively, low  $\delta^{15}\text{N}$  could suggest nitrate levels become so low  
294 that the heavy  $\delta^{15}\text{N}$  of the residual nitrate can no longer dominate the isotopic composition  
295 of biomass. As the thermocline deepened during the Early Triassic hothouse, nitrate supply  
296 from deep-water environments to the euphotic zone had to overcome the density barrier,  
297 and this could only be achieved by diffusion (Fig. 2C). Diffusion would eventually have  
298 drained the nitrate inventory of deep-water reservoirs. In open water settings, nitrate  
299 consumption exceeding nitrate production was probably a protracted process, controlled

300 by the evolution and intensity of ocean anoxia. This is consistent with the observed  
301 prolonged and gradual  $\delta^{15}\text{N}$  decrease from the earliest Triassic to the S-S boundary (Grasby  
302 et al., 2016). Localized depletion of nitrate on some isolated platforms, marked by  $\delta^{15}\text{N}$   
303 falling to  $\sim 0$  ‰, occurred much earlier at the P-T boundary (Fig. 5); this was probably due  
304 to a lack of nitrate resupply from the deep reservoirs in such settings.

305         The near-antithetic relationship between  $\delta^{15}\text{N}$  and the  $\text{C}/\text{N}_{\text{atomic}}$  ratio at the S-S  
306 transition suggests that a common cause simultaneously drove  $\delta^{15}\text{N}$  to lower values and  
307 the  $\text{C}/\text{N}_{\text{atomic}}$  ratio to higher values (and vice versa). This is unlikely to be due to the input of  
308 terrestrial organic matter (which typically has low  $\delta^{15}\text{N}$  and high  $\text{C}/\text{N}_{\text{atomic}}$  ratios) because,  
309 with the near-extinction of land plants at the end of the Permian and the subsequent low  
310 terrestrial biomass on Pangea (Looy et al., 1999), terrestrial N input is unlikely to have  
311 affected the isotopic composition of the oceanic N pool. Instead, the factor that drove the  
312  $\delta^{15}\text{N}$  and  $\text{C}/\text{N}_{\text{atomic}}$  ratio in opposite directions was probably the bioavailability of nitrate. In  
313 the case of low nitrate availability and long-term anoxia, nitrate-removal processes utilize  
314 nitrate and the corresponding isotopic fractionation effects decrease while nitrogen  
315 fixation is enhanced thereby compensating for the nutrient-N loss. Both processes lower  
316  $\delta^{15}\text{N}$  values of organic N. At the same time, anoxia enhances bacterial recycling of N-rich  
317 amino acids from organic matter (Van Mooy et al., 2002), leading to a more intense loss of  
318 sedimentary N during diagenesis and higher  $\text{C}/\text{N}_{\text{atomic}}$  ratios.

319         Low sulphate concentrations and episodic euphotic zone euxinia characterize the  
320 Early Triassic oceans (Grice et al., 2005; Song et al., 2014). These are largely, or at least  
321 partially, due to enhanced bacterial sulphate reduction, perhaps due to high marine  
322 productivity (Schobben et al., 2015). However, with increasing water column  $\text{O}_2$  deficiency,

323 heterotrophic bacteria favour energy extraction pathways with high yields. Sulphate  
324 reduction ranks low in this respect amongst anaerobic respiration (Table 1) and is only  
325 favoured once nitrate is depleted (Altabet, 2006). We thus argue that enhanced sulphate  
326 reduction in the Early Triassic oceans was probably a response to a functional shift in  
327 microbial communities from nitrate consuming ( $\Delta G^0 = -445$  kJ/mol C) to sulphate  
328 consuming ( $\Delta G^0 = -61$  kJ/mol C) and thus did not necessarily require eutrophication  
329 (Schobben et al., 2016).

### 330 *6.3 Enhanced nitrogen fixation, Mo limitation and a shift in nutrient-N inventory*

331 The protracted anoxic conditions in the Early Triassic promoted nitrogen fixation.  
332 The  $\delta^{15}\text{N}$  values of  $\sim 0.5$  to  $-1$  ‰ at Jiarong and Xiakou suggest  $\text{N}_2$  fixation dominated  
333 equatorial oceans. A similar scenario is suggested for Cretaceous oceanic anoxic events  
334 when comparably low  $\delta^{15}\text{N}$  values are associated with black shale deposition (Junium and  
335 Arthur, 2007), highlighting a key role of diazotrophs (nitrogen fixers) under anoxic  
336 conditions.

337 Biological nitrogen fixation is an enzyme-catalyzed  $\text{N}_2$  reduction, which has low  
338 energy yields ( $\Delta G^0 = -157$  kJ/mol N) and has to overcome a large kinetic barrier to break  
339 three N-N bonds in the  $\text{N}_2$  molecule (Altabet, 2006). This can only be achieved by  
340 diazotrophs that are exclusively prokaryotes. Most diazotrophs are anaerobic bacteria or  
341 archaea except for diazotrophic cyanobacteria which have special cell walls that inhibit  
342 oxygen diffusion (Altabet, 2006). This is because the nitrogenase enzyme has a metal  
343 center consisting of either Mo-Fe, V-Fe or Fe-only complexes and its function is irreversibly  
344 inhibited by free oxygen (Berman-Frank et al., 2003). Thus, diazotrophs generally prefer  
345 anoxic environments, require P as a nutrient, and metal ions for synthesizing the

346 nitrogenase enzyme. Phosphorus availability may not have been a limiting factor in the  
347 Early Triassic ocean because of 1) increased terrestrial P input via enhanced weathering; 2)  
348 recycling of P from anoxic sediments; and 3) reduced metazoan uptake following  
349 extinctions of shelly fossils that incorporated P in CaCO<sub>3</sub> shells and biogenic apatite. This  
350 inference is supported by data from Jiarong, where P and Al contents are positively  
351 correlated ( $r = 0.77, p < 0.05$ ) but not as significantly as Fe vs. Al ( $r = 0.96, p < 0.05$ ) and V  
352 vs. Al ( $r = 0.95, p < 0.05$ ) (Fig. 6), suggesting P sources were not entirely terrestrial.

353         Metabolizable trace metals Mo(VI), V(V) and Fe(II) are redox-sensitive and they can  
354 be scavenged from the water column into sediments under intensely anoxic and euxinic  
355 conditions. A scarcity of such trace nutrients could severely suppress nitrogen fixation,  
356 leading to a pause in nitrogen cycling after nitrate depletion and a consequent collapse in  
357 oceanic productivity (Fig. 1, model C). However, such a scenario seemingly did not occur, at  
358 least not globally or for the long term, in the Early Triassic. This is probably because Fe(II)  
359 availability was sufficiently high, being reduced from Fe oxides from riverine input and  
360 aeolian dust or directly derived from hydrothermal activity at mid-ocean ridges. High Fe(II)  
361 availability is consistent with the development of ferruginous conditions (Clarkson et al.,  
362 2016) and the global abundance of pyrite framboids in Early Triassic sediments (Wignall  
363 and Twitchett, 2002).

364         In contrast, the Mo reservoir was probably much smaller than the Fe reservoir with  
365 minor input into large sinks, and could be depleted more easily. However, Mo availability  
366 cannot be easily evaluated because Mo tends to sink in sediments under anoxic-euxinic  
367 conditions. Thus Mo concentration measured from sedimentary rocks mainly reflects water  
368 column redox changes and does not necessarily mirror Mo availability in seawater. A

369 | proper estimation would require multiple speculations on Mo input and sink. Mo limitation  
370 | in this case is inferred from indirect evidence from  $\delta^{15}\text{N}$ . Mo-Fe nitrogenase is much more  
371 | efficient than V-Fe and Fe-only nitrogenase (Berman-Frank et al., 2003). A shift in  
372 | nitrogenase type leads to a change in the isotopic fractionation during nitrogen fixation  
373 | ( $^{14}\text{N}$  is preferably used) which could have resulted in more negative values in sedimentary  
374 |  $\delta^{15}\text{N}$  (Zhang et al., 2014). The sporadic development of more negative  $\delta^{15}\text{N}$  values ( $< -2$  ‰)  
375 | in the Jiarong section might have been a manifestation of short pulses of Mo limitation.  
376 | Alternatively, (or collectively), these low  $\delta^{15}\text{N}$  values may also be explained by partial  $\text{NH}_4^+$   
377 | uptake. Low  $\delta^{15}\text{N}$  values are comparably rare throughout Earth's history, including the  
378 | Precambrian, where Mo was likely much less abundant than at any time in the Phanerozoic  
379 | (Stüeken et al., 2016). However,  $\delta^{15}\text{N}$  values  $< -2$  ‰ are seen during intensive anoxia, such  
380 | as during the oceanic anoxic events in the early Jurassic and middle Cretaceous (Jenkyns et  
381 | al., 2001; Junium and Arthur, 2007), suggesting Mo limitation and/or  $\text{NH}_4^+$ -rich conditions  
382 | may have occurred more frequently than previously thought.

383 | Nitrate (including nitrite) and ammonium (including ammonia) are two end  
384 | members of oceanic nutrient-N (Fig. 1). In oxic waters, nitrification actively converts  $\text{NH}_4^+$   
385 | to  $\text{NO}_3^-$ . Many primary producers rely on the nitrate supply from deep waters, brought up  
386 | by mixing and upwelling (Fig. 2C). In contrast, in anoxic oceans, anammox, denitrification  
387 | and dissimilatory nitrate reduction to ammonium (DNRA) compete for nitrate for high  
388 | anaerobic energy yields (Fig.1; Table 1). Anammox consumes both  $\text{NH}_4^+$  and  $\text{NO}_2^-$  and  
389 | produces non-nutritious  $\text{N}_2$ . In the case of intense anoxia (e.g., fast expansion of OMZ) and  
390 | especially euxinia, DNRA produces an electron sink and thus outcompetes denitrification  
391 | for nitrate (An and Gardner, 2002; Giblin et al., 2013) (Table 1). Such conditions, typically

392 accompanied by high temperatures, high organic carbon burial and sulphate reduction  
393 rates, are seen in polluted coastal environments today but were likely widespread in the  
394 Early Triassic oceans, especially during the P-T transition and in the late Smithian (Grasby  
395 et al., 2012; Sun et al., 2012; Schobben et al., 2015; Sun et al., 2015). Unlike denitrification  
396 and anammox, DNRA recycles nitrate to bioavailable  $\text{NH}_4^+$ . A combination of nitrate net  
397 consumption and enhanced nitrogen fixation and DNRA likely led to a shift from a  $\text{NO}_3^-$   
398 dominated nutrient-N inventory to one dominated by  $\text{NH}_4^+$  (Fig. 1, models B and C; Fig. 8).  
399 Though  $\text{NH}_4^+$  dominance does not necessarily result in  $\text{NH}_4^+$  accumulation to high  
400 concentrations. Once established, the only pathway to reverse this shift is through  
401 nitrification, which is a light-sensitive aerobic reaction (Zehr and Ward, 2002), thus  
402 requiring oxygenation of deeper (dark) waters.

#### 403 *6.4 Comparison with the modern Black Sea and the heterogeneity of Early Triassic oceans*

404 The Black Sea is the world's largest anoxic basin and a contemporary analogue for  
405 an ammonium ocean that can be used to test our conceptual model. The  $\text{NH}_4^+$   
406 concentration in the Black Sea is  $\sim 0 \mu\text{M}$  in oxygenated surface waters but increases  
407 significantly with depth and oxygen deficiency to  $\sim 30 \mu\text{M}$  at 250 m depth while nitrate  
408 concentration remains  $\sim 0 \mu\text{M}$  below the suboxic-anoxic interface (Fig. 7; Kuypers et al.,  
409 2003). Our model fits these observations— nitrate is depleted while ammonium  
410 accumulates in anoxic environments (Fig. 1 model B).

411 Accumulation of  $\text{NH}_4^+$  in the Black Sea is at least partially due to strong stratification  
412 of the water column (Fig. 7). The freshwater discharge from the Danube and other rivers  
413 creates an oxic cap that prevents water column mixing. Though not a perfect analogue, the  
414 P-T oceans are also generally considered to be highly stratified due to extreme hothouse

415 climate and stagnation of ocean circulations (e.g., Hotinski et al., 2001; Winguth et al.,  
416 2015).

417 In contrast to Black Sea surface waters, where nitrate still exists, low latitude  
418 shallow-water Early Triassic  $\delta^{15}\text{N}$  values fall to  $\sim 0$  ‰ and lower immediately above the P-  
419 T boundary (Luo et al., 2011) and at the S-S transition, which suggests the nutrient-N  
420 supply to surface waters was composed entirely of newly fixed-N. This was probably due to  
421 intense photic zone euxinia (Grice et al., 2005; Cao et al., 2009) which inhibited nitrification  
422 in the surface water. In contrast,  $\delta^{15}\text{N}$  values from northern higher latitudes (e.g.,  
423 Vindodden) have a mixed signature of N-fixation and nitrate. The presence of nitrate  
424 suggests nitrification was still partially active in these settings at night, in the winter  
425 and/or in the oxygenated lower euphotic zone.

#### 426 *6.5 Ammonium fertilization*

427 Marine phytoplankton and newly generated organic matter have a near-constant  
428 stoichiometric composition ratio — C:N:P = 106:16:1, known as the Redfield ratio. The  
429 Redfield stoichiometry suggests a higher demand for nutrient-N than P amongst primary  
430 producers. At higher temperatures, eukaryotic phytoplankton have a reduced demand for P  
431 required for cellular protein synthesis and shifts the oceanic nutrient structure to one that  
432 is N-limited (Toseland et al., 2013). Diazotrophic cyanobacteria are uniquely suited to such  
433 environments due to their self-sufficiency in nutrient-N. The recycling of cyanobacterial  
434 biomass occurs rapidly during heterotrophy in the euphotic zone, releasing  $\text{NH}_4^+$  that can  
435 be assimilated by other phytoplankton (Fulton et al., 2012). Such processes could continue  
436 to the point that P is consumed in the euphotic zone and then becomes the limiting  
437 nutrient. Given this constraint and the lack of major shifts in the Redfield N/P ratio in the

438 Early Triassic (Grasby et al., 2016), the size of the ancient deep ocean  $\text{NH}_4^+$  reservoir could  
439 not have been much greater than the modern ocean nitrate reservoir. This suggests an  
440 Early Triassic deep ocean  $\text{NH}_4^+$  concentration was unlikely to have been greater than  $\sim 50$   
441  $\mu\text{M}$ .

442 Phytoplankton (both eukaryotes and cyanobacteria) generally prefer  $\text{NH}_4^+$  to  $\text{NO}_3^-$  as  
443 a nutrient source, because of the redundant energy costs expended when reducing  $\text{NO}_3^-$  to  
444  $\text{NH}_4^+$  (Zehr and Ward, 2002). The exception is diatoms which generally prefer  $\text{NO}_3^-$  as a  
445 nutrient-N source but they only appeared in the Jurassic. One contemporary example for  
446  $\text{NH}_4^+$  fertilization is the long-lasting Texas Brown Tide at the Laguna Madre/Baffin Bay  
447 estuary, caused by the alga *Aureomonas lagunensis*. This species is able to use  $\text{NH}_4^+$  or  $\text{NO}_2^-$   
448 but not  $\text{NO}_3^-$  and its enduring bloom was fertilized by  $\text{NH}_4^+$  produced by DNRA in an  
449 environment with high sulphide concentrations (An and Gardner, 2002). Similarly, regional  
450 primary productivity increase and stromatolite development (e.g. Pruss et al., 2006; Chen  
451 et al., 2014) in the Early Triassic were likely stimulated by  $\text{NH}_4^+$  fertilization. The extensive  
452 microbialite build-ups in the aftermath of end-Permian mass extinction (Fig. 2A, B) were  
453 probably constructed by diazotrophs ( $\text{NH}_4^+$  self-sufficient by N-fixation), or otherwise  
454 fertilized by ambient  $\text{NH}_4^+$ . The onset of microbialite development in the earliest  
455 Griesbachian clearly coincided with enhanced nitrogen fixation (Cao et al., 2009; Xie et al.,  
456 2010; Luo et al., 2011) — a feature also seen during the S-S transition. The bloom of  
457 prasinophyte algae immediately after the end-Permian mass extinction while N-fixation by  
458 cyanobacteria was occurring, is suggested to have provided prasinophytes with  $\text{NH}_4^+$  in  
459 nutrient-limited environments (Jia et al., 2012). The demise of microbialites towards the  
460 Middle Triassic (Fig. 2B) was likely due to a general amelioration of environmental stresses

461 and the re-establishment of potent nitrification, reducing  $\text{NH}_4^+$  during deep-water re-  
462 oxygenation (Fig. 1, model A).

### 463 *6.6 Ammonium intoxication*

464         Although it fertilizes phytoplankton,  $\text{NH}_4^+$  is a major metabolic waste and can be  
465 lethal to both animals and higher plants at high concentrations (Britto and Kronzucker,  
466 2002).  $\text{NH}_4^+$  accumulation, for instance, is a widespread problem in modern fish farming.  
467 Terrestrial animals and birds convert  $\text{NH}_4^+$  to the much less toxic urea but aquatic animals  
468 generally rely on direct excretion of  $\text{NH}_4^+$  to ambient water (Ip et al., 2001). The lethal  
469 concentration of ammonium for a wide range of marine vertebrates is  $12.5 \mu\text{M}$  (Knoph and  
470 Thorud, 1996; U.S. Environmental Protection Agency, 1998), much lower than the  $\sim 50 \mu\text{M}$   
471 maximum estimated for the Early Triassic oceans. In general, invertebrates are more  
472 tolerant to ammonia (i.e., total ammonia =  $\text{NH}_4^+$  and  $\text{NH}_3$ ) than vertebrates while  
473 freshwater animals are more tolerant than marine animals. The toxicity of total ammonia  
474 manifests as damage to the central nervous system in vertebrates and is amplified at higher  
475 pH (e.g., in seawater). This is because  $\text{NH}_4^+$  is more toxic but less diffusive while most  
476 animal membranes are more permeable to  $\text{NH}_3$  (Ip et al., 2001). Remineralization of  
477 organic N in anoxic environments exclusively leads to  $\text{NH}_4^+$  and  $\text{NH}_3$  accumulation (Fig. 1,  
478 models B and C). Since protein decay is independent of redox conditions, and nitrification is  
479 inhibited in anoxic waters, degradation of organic remains and diazotrophs could have, at  
480 least in short term, produced excessive  $\text{NH}_4^+$  that may, at least in part, explain the hitherto  
481 enigmatic Early Triassic extinction/changeover events amongst nekton such as conodonts  
482 and fish. Such groups would be somewhat immune to the typical end-Permian scenario of  
483 high temperatures and low oxygen levels due to their ability to migrate to higher latitudes

484 and their upper water column habitats. Neither factor would help nekton escape  $\text{NH}_4^+$ - $\text{NH}_3$   
485 poisoning. Even at modest increases in concentrations, the swimming ability of animals  
486 such as fish is impaired (Ip et al., 2001).

487 On the other hand, cephalopods are exclusively carnivores with fast growth rates for  
488 most of their life cycle. They have a high demand for proteins and the dominance of amino  
489 acid metabolism leads to a high  $\text{NH}_4^+$  accumulation in their systems (Lee, 1995). Some  
490 groups of cephalopods have much high tolerance of  $\text{NH}_4^+$  because they retain this  
491 metabolic waste in their tissues to achieve neutral buoyancy while other groups did not  
492 develop this physiological mechanism, but instead transform toxic  $\text{NH}_4^+$  to  $\text{N}_2$  gas (e.g.,  
493 *Nautilus*) or develop jelly-like chloride compounds to maintain buoyancy (Voight et al.  
494 1995). Thus, the fast turnover of ammonoids during the end-Permian mass extinction may  
495 reflect the success of those groups with a tolerance for high  $\text{NH}_4^+$  concentrations.  $\text{NH}_4^+$   
496 levels in ammonoid soft tissue were probably often high and the post mortem release  
497 during burial maintains high ambient pH levels thus inhibiting calcium phosphate  
498 replacement (Clements et al., 2017). This likely explains why ammonoid soft body tissue is  
499 rarely seen in fossil Lagerstätte.

500 Ammonium concentrations are not recorded in sedimentary rocks. Quantitative  
501 Earth system modelling studies are needed to better constrain the concentration of total  
502 ammonia in the P-T oceans and to further validate this hypothesis. If correct, ammonium  
503 poisoning is a previously unidentified end-Permian and Early Triassic killing mechanism  
504 (Fig. 8) and, once accumulated, its removal from seawater is difficult under anoxic and  
505 stratified oceanic conditions.

506 *6.8 Loss of dissolved nutrient-N in anoxic waters*

507 Since nitrification can occur at low oxygen concentrations, establishment of  
508 ammonium oceans in the Phanerozoic could only occur in highly stratified oceans and  
509 during intensive ocean anoxic events. In cases of moderately anoxic conditions or fast  
510 oscillations in (dys)oxic and anoxic conditions, ammonium is likely converted to nitrate,  
511 which would then be denitrified. Additionally, as observed in OMZs in contemporary Omani  
512 Shelf, offshore Peru and elsewhere, DNRA and anammox bacteria can form DNRA-  
513 Anammox coupling and account for nutrient-N losses in areas of no detectable  
514 denitrification (Jensen et al., 2011). These processes could result in losses of both  
515 ammonium and nitrate, leading to a decrease in dissolved inorganic nutrient-N inventory  
516 (Fig. 8).

517

## 518 **7. Conclusion**

519 Assertions that primary productivity in the Early Triassic oceans was either  
520 universally high or universally low are both untenable. The transition from nitrate oceans  
521 to ammonium oceans was accompanied by decreases in both the respiration efficiency of  
522 organisms and in the oceanic nutrient-N reservoir (Fig. 8). Though controlled by regional  
523 redox and oceanographic setting,  $\text{NH}_4^+$  could temporarily and regionally boost primary  
524 productivity although it was probably low in general since most nutrient-N was likely lost  
525 during persistent periods of anoxia. Enhanced sulphate reduction, which is widely implied  
526 in the P-T oceans, could be attributed to a functional shift in microbial communities from  
527 nitrate consumption to sulphate consumption in a nitrate-starved ocean and thus does not  
528 necessarily require eutrophication.

529 Ammonium intoxication is one of the worst case scenarios of ammonium ocean  
530 which, in turn, is likely a synergetic effect of widespread ocean anoxia and intensive water  
531 column stratification. Though remaining conceptual and awaiting Earth system modelling  
532 studies to further constrain, ammonia toxicity has not been considered in geological  
533 studies, and yet it may have played a substantial role in suppressing complex life before the  
534 rise of oxygen and probably in selectivity during many past extinctions.

535  
536 **Acknowledgments:** This is a contribution to DFG (German Science Foundation) Research  
537 Unit TERSANE (FOR 2332: Temperature-related stressors as a unifying principle in ancient  
538 extinctions; Project Jo 219/15). National Natural Science Foundation of China (41821001,  
539 41602026, 41602016), the National Key R&D Program of China (2016YFA0601104), and  
540 Natural Environment Research Council of UK (RG.EVEA.109961; NE/J01799X/1)  
541 financially supported this study. Editor T. Mather is thanked for professional handling.  
542 Constructive comments from E. Stüeken and two anonymous reviewers improved this  
543 paper. K. De Baets [and C. Scotese are](#) thanked for fruitful discussions.

544  
545 **References**

546 Algeo, T.J., Chen, Z.Q., Fraiser, M.L., Twitchett, R.J., 2011. Terrestrial-marine teleconnections in the  
547 collapse and rebuilding of Early Triassic marine ecosystems. *Palaeogeogr. Palaeoclimatol.*  
548 *Palaeoecol.* 308, 1-11.

549 Altabet, M.A., 2006. Isotopic tracers of the marine nitrogen cycle: Present and past, in: Volkman, J.K.  
550 (Ed.), *Marine Organic Matter: Biomarkers, Isotopes and DNA*. Springer Berlin Heidelberg,  
551 Berlin, Heidelberg, pp. 251-293.

552 Altabet, M.A., 2007. Constraints on oceanic N balance/imbalance from sedimentary <sup>15</sup>N records.  
553 *Biogeosciences* 4, 75-86.

554 An, S., Gardner, W.S., 2002. Dissimilatory nitrate reduction to ammonium (DNRA) as a nitrogen link,  
555 versus denitrification as a sink in a shallow estuary (Laguna Madre/Baffin Bay, Texas).  
556 *Marine Ecology Progress Series* 237, 41-50.

- 557 Berman-Frank, I., Lundgren, P., Falkowski, P., 2003. Nitrogen fixation and photosynthetic oxygen  
558 evolution in cyanobacteria. *Research in Microbiology* 154, 157-164.
- 559 Bottjer, D.J., Clapham, M.E., Fraiser, M.L., Powers, C.M., 2008. Understanding mechanisms for the  
560 end-Permian mass extinction and the protracted Early Triassic aftermath and recovery.  
561 *GSA Today* 18, 4-10.
- 562 Bristow, L.A., Dalsgaard, T., Tiano, L., Mills, D.B., Bertagnolli, A.D., Wright, J.J., Hallam, S.J., Ulloa, O.,  
563 Canfield, D.E., Revsbech, N.P., Thamdrup, B., 2016. Ammonium and nitrite oxidation at  
564 nanomolar oxygen concentrations in oxygen minimum zone waters. *Proc Natl Acad Sci U S*  
565 *A* 113, 10601-10606.
- 566 Britto, D.T., Kronzucker, H.J., 2002.  $\text{NH}_4^+$  toxicity in higher plants: a critical review. *Journal of Plant*  
567 *Physiology* 159, 567-584.
- 568 Cao, C., Love, G.D., Hays, L.E., Wang, W., Shen, S., Summons, R.E., 2009. Biogeochemical evidence for  
569 euxinic oceans and ecological disturbance presaging the end-Permian mass extinction  
570 event. *Earth Planet. Sci. Lett.* 281, 188-201.
- 571 Chen, Y., Jiang, H., Lai, X., Yan, C., Richoz, S., Liu, X., Wang, L., 2015. Early Triassic conodonts of  
572 Jiarong, Nanpanjiang Basin, southern Guizhou Province, South China. *J. Asian Earth Sci.*  
573 105, 104-121.
- 574 Chen, Z.-Q., Wang, Y., Kershaw, S., Luo, M., Yang, H., Zhao, L., Feng, Y., Chen, J., Yang, L., Zhang, L.,  
575 2014. Early Triassic stromatolites in a siliciclastic nearshore setting in northern Perth  
576 Basin, Western Australia: Geobiologic features and implications for post-extinction  
577 microbial proliferation. *Global Planet. Change* 121, 89-100.
- 578 Clarkson, M.O., Wood, R.A., Poulton, S.W., Richoz, S., Newton, R.J., Kasemann, S.A., Bowyer, F.,  
579 Krystyn, L., 2016. Dynamic anoxic ferruginous conditions during the end-Permian mass  
580 extinction and recovery. *Nature Communications* 7, 12236.
- 581 Clements, T., Colleary, C., De Baets, K., Vinther, J., 2017. Buoyancy mechanisms limit preservation of  
582 coleoid cephalopod soft tissues in Mesozoic Lagerstätten. *Palaeontology* 60, 1-14.
- 583 Elrick, M., Polyak, V., Algeo, T.J., Romaniello, S., Asmerom, Y., Herrmann, A.D., Anbar, A.D., Zhao, L.,  
584 Chen, Z.-Q., 2017. Global-ocean redox variation during the middle-late Permian through  
585 Early Triassic based on uranium isotope and Th/U trends of marine carbonates. *Geology*  
586 45, 163-166.
- 587 Feely, R.A., Trefry, J.H., Massoth, G.J., Metz, S., 1991. A comparison of the scavenging of phosphorus  
588 and arsenic from seawater by hydrothermal iron oxyhydroxides in the Atlantic and Pacific  
589 Oceans. *Deep Sea Research Part A. Oceanographic Research Papers* 38, 617-623.
- 590 Fulton, J.M., Arthur, M.A., Freeman, K.H., 2012. Black Sea nitrogen cycling and the preservation of  
591 phytoplankton  $\delta^{15}\text{N}$  signals during the Holocene. *Global Biogeochem. Cycles* 26, GB2030.
- 592 Giblin, A., Tobias, C., Song, B., Weston, N., Banta, G., Rivera-Monroy, V., 2013. The importance of  
593 dissimilatory nitrate reduction to ammonium (DNRA) in the nitrogen cycle of coastal  
594 ecosystems. *Oceanography* 26, 124-131.
- 595 Grasby, S.E., Beauchamp, B., Embry, A., Sanei, H., 2012. Recurrent Early Triassic ocean anoxia.  
596 *Geology* 41, 175-178.
- 597 Grasby, S.E., Beauchamp, B., Knies, J., 2016. Early Triassic productivity crises delayed recovery from  
598 world's worst mass extinction. *Geology* 44, 779-782.

- 599 Grice, K., Cao, C., Love, G.D., Böttcher, M.E., Twitchett, R.J., Grosjean, E., Summons, R.E., Turgeon, S.C.,  
600 Dunning, W., Jin, Y., 2005. Photic zone euxinia during the Permian-Triassic superanoxic  
601 event. *Science* 307, 706-709.
- 602 Guerrero, M.A., Jones, R.D., 1996. Photoinhibition of marine nitrifying bacteria. I. Wavelength-  
603 dependent response. *Marine Ecology Progress Series* 141, 183-192.
- 604 Hotinski, R.M., Bice, K.L., Kump, L.R., Najjar, R.G., Arthur, M.A., 2001. Ocean stagnation and end-  
605 Permian anoxia. *Geology* 29, 7-10.
- 606 Hounslow, M.W., Hu, M., Mørk, A., Weitschat, W., Vigran, J.O., Karloukovski, V., Orchard, M.J., 2008.  
607 Intercalibration of Boreal and Tethyan time scales: the magnetobiostratigraphy of the  
608 Middle Triassic and the latest Early Triassic from Spitsbergen, Arctic Norway. *Polar*  
609 *Research* 27, 469-490.
- 610 Hulth, S., Aller, R.C., Gilbert, F., 1999. Coupled anoxic nitrification/manganese reduction in marine  
611 sediments. *Geochim. Cosmochim. Acta* 63, 49-66.
- 612 Ip, Y.K., Chew, S.F., Randall, D.J., 2001. Ammonia toxicity, tolerance, and excretion. *Fish Physiology*  
613 20, 109-148.
- 614 Jenkyns, H.C., Gröcke, D.R., Hesselbo, S.P., 2001. Nitrogen isotope evidence for water mass  
615 denitrification during the Early Toarcian (Jurassic) oceanic anoxic event.  
616 *Paleoceanography* 16, 593-603.
- 617 Jensen, M.M., Lam, P., Revsbech, N.P., Nagel, B., Gaye, B., Jetten, M.S.M., Kuypers, M.M.M., 2011.  
618 Intensive nitrogen loss over the Omani Shelf due to anammox coupled with dissimilatory  
619 nitrite reduction to ammonium. *The Isme Journal* 5, 1660.
- 620 Jia, C., Huang, J., Kershaw, S., Luo, G., Farabegoli, E., Perri, M.C., Chen, L., Bai, X., Xie, S., 2012.  
621 Microbial response to limited nutrients in shallow water immediately after the end-  
622 Permian mass extinction. *Geobiology* 10, 60-71.
- 623 Junium, C.K., Arthur, M.A., 2007. Nitrogen cycling during the Cretaceous, Cenomanian-Turonian  
624 Oceanic Anoxic Event II. *Geochemistry Geophysics Geosystems* 8, Q03002.
- 625 Kidder, D.L., Worsley, T.R., 2010. Phanerozoic Large Igneous Provinces (LIPs), HEATT (Haline  
626 Euxinic Acidic Thermal Transgression) episodes, and mass extinctions. *Palaeogeogr.*  
627 *Palaeoclimatol. Palaeoecol.* 295, 162-191.
- 628 Knies, J., Grasby, S.E., Beauchamp, B., Schubert, C.J., 2013. Water mass denitrification during the  
629 latest Permian extinction in the Sverdrup Basin, Arctic Canada. *Geology* 41, 167-170.
- 630 Knoph, M.B., Thorud, K., 1996. Toxicity of ammonia to Atlantic salmon (*Salmo salar* L.) in  
631 seawater—Effects on plasma osmolality, ion, ammonia, urea and glucose levels and  
632 hematologic parameters. *Comparative Biochemistry and Physiology Part A: Physiology*  
633 113, 375-381.
- 634 Konovalov, S.K., Murray, J.W., Luther III, G.W., 2005. Basic processes of Black Sea biogeochemistry.  
635 *Oceanology* 18, 24-35.
- 636 Kump, L.R., Pavlov, A., Arthur, M.A., 2005. Massive release of hydrogen sulfide to the surface ocean  
637 and atmosphere during intervals of oceanic anoxia. *Geology* 33, 397-400.
- 638 Kuypers, M.M.M., Sliemers, A.O., Lavik, G., Schmid, M., Jørgensen, B.B., Kuenen, J.G., Sinninghe  
639 Damsté, J.S., Strous, M., Jetten, M.S.M., 2003. Anaerobic ammonium oxidation by anammox  
640 bacteria in the Black Sea. *Nature* 422, 608.

- 641 Lam, P., Jensen, M.M., Lavik, G., McGinnis, D.F., Müller, B., Schubert, C.J., Amann, R., Thamdrup, B.,  
642 Kuypers, M.M.M., 2007. Linking crenarchaeal and bacterial nitrification to anammox in the  
643 Black Sea. *Proceedings of the National Academy of Sciences* 104, 7104-7109.
- 644 Lee, P.G., 1995. Nutrition of cephalopods: Fueling the system. *Marine and Freshwater Behaviour*  
645 *and Physiology* 25, 35-51.
- 646 Lehrmann, D.J., Payne, J.L., Felix, S.V., Dillett, P.M., Wang, H., Yu, Y.Y., Wei, J.Y., 2003. Permian-  
647 Triassic Boundary Sections from Shallow-Marine Carbonate Platforms of the Nanpanjiang  
648 Basin, South China: Implications for Oceanic Conditions Associated with the End-Permian  
649 Extinction and Its Aftermath. *Palaios* 18, 138-152.
- 650 Looy, C.V., Brugman, W.A., Dilcher, D.L., Visscher, H., 1999. The delayed resurgence of equatorial  
651 forests after the Permian-Triassic ecologic crisis. *Proc. Natl. Acad. Sci. U.S.A.* 96, 13857-  
652 13862.
- 653 Luo, G.M., Wang, Y.B., Algeo, T.J., Kump, L.R., Bai, X., Yang, H., Yao, L., Xie, S.C., 2011. Enhanced  
654 nitrogen fixation in the immediate aftermath of the latest Permian marine mass extinction.  
655 *Geology* 39, 647-650.
- 656 McCready, R.G.L., Gould, W.D., Barendregt, R.W., 1983. Nitrogen isotope fractionation during the  
657 reduction of  $\text{NO}_3^-$  to  $\text{NH}_4^+$  by *Desulfovibrio* sp. *Canadian Journal of Microbiology* 29, 231-  
658 234.
- 659 Meyer, K.M., Kump, L.R., Ridgwell, A., 2008. Biogeochemical controls on photic-zone euxinia during  
660 the end-Permian mass extinction. *Geology* 36, 747-750.
- 661 Mørk, A., Elvebakk, G., Forsberg, A.W., Hounslow, M.W., Nakrem, h.A., Vigran, J.O., Weitschat, W.,  
662 1999. The type section of the Vikinghøgda Formation: a new Lower Triassic unit in central  
663 and eastern Spitsbergen. *Polar Research* 18, 51-82.
- 664 Payne, J.L., Lehrmann, D.J., Wei, J.Y., Orchard, M.J., Schrag, D.P., Knoll, A.H., 2004. Large perturbations  
665 of the carbon cycle during recovery from the End-Permian extinction. *Science* 305, 506-  
666 509.
- 667 Penn, J.L., Deutsch, C., Payne, J.L., Sperling, E.A., 2018. Temperature-dependent hypoxia explains  
668 biogeography and severity of end-Permian marine mass extinction. *Science* 362, eaat1327.
- 669 Pruss, S.B., Bottjer, D.J., Corsetti, F.A., Baud, A., 2006. A global marine sedimentary response to the  
670 end-Permian mass extinction: Examples from southern Turkey and the western United  
671 States. *Earth-Sci. Rev.* 78, 193-206.
- 672 Quan, T.M., Falkowski, P.G., 2009. Redox control of N:P ratios in aquatic ecosystems. *Geobiology* 7,  
673 124-139.
- 674 Rabalais, N.N., Turner, R.E., Wiseman, W.J., 2002. Gulf of Mexico Hypoxia, a.k.a. "The Dead Zone".  
675 *Annual Review of Ecology and Systematics* 33, 235-263.
- 676 Schobben, M., Stebbins, A., Ghaderi, A., Strauss, H., Korn, D., Korte, C., 2015. Flourishing ocean drives  
677 the end-Permian marine mass extinction. *Proceedings of the National Academy of Sciences*  
678 112, 10298-10303.
- 679 Schobben, M., Stebbins, A., Ghaderi, A., Strauss, H., Korn, D., Korte, C., 2016. Eutrophication,  
680 microbial-sulfate reduction and mass extinctions. *Communicative & Integrative Biology* 9,  
681 e1115162.

- 682 Schoepfer, S.D., Henderson, C.M., Garrison, G.H., Ward, P.D., 2012. Cessation of a productive coastal  
683 upwelling system in the Panthalassic Ocean at the Permian–Triassic Boundary.  
684 *Palaeogeogr. Palaeoclimatol. Palaeoecol.* 313-314, 181-188.
- 685 Scotese, C.R., Moore, T.L., 2014. Atlas of Phanerozoic Ocean Currents and Salinity (Mollweide  
686 Projection), PALEOMAP Project PaleoAtlas for ArcGIS, PALEOMAP Project, Evanston,  
687 Illinois.
- 688 Sigman, D., Karsh, K., Casciotti, K., 2009. Ocean process tracers: nitrogen isotopes in the ocean,  
689 *Encyclopedia of Ocean Science*, 2nd edition. Elsevier, Amsterdam, pp. 4138-4153.
- 690 Smith, J.M., Chavez, F.P., Francis, C.A., 2014. Ammonium Uptake by Phytoplankton Regulates  
691 Nitrification in the Sunlit Ocean. *PLoS ONE* 9, e108173.
- 692 Song, H., Tong, J., Algeo, T.J., Song, H., Qiu, H., Zhu, Y., Tian, L., Bates, S., Lyons, T.W., Luo, G., Kump,  
693 L.R., 2014. Early Triassic seawater sulfate drawdown. *Geochim. Cosmochim. Acta* 128, 95-  
694 113.
- 695 Stüeken, E.E., Kipp, M.A., Koehler, M.C., Buick, R., 2016. The evolution of Earth's biogeochemical  
696 nitrogen cycle. *Earth-Sci. Rev.* 160, 220-239.
- 697 Sun, Y.D., Joachimski, M.M., Wignall, P.B., Yan, C.B., Chen, Y.L., Jiang, H.S., Wang, L.N., Lai, X.L., 2012.  
698 Lethally hot temperatures during the Early Triassic greenhouse. *Science* 338, 366-370.
- 699 Sun, Y.D., Wignall, P.B., Joachimski, M.M., Bond, D.P.G., Grasby, S.E., Sun, S., Yan, C.B., Wang, L.N.,  
700 Chen, Y.L., Lai, X.L., 2015. High amplitude redox changes in the late Early Triassic of South  
701 China and the Smithian/Spathian extinction. *Palaeogeogr. Palaeoclimatol. Palaeoecol.* 427,  
702 62-78.
- 703 Toseland, A., Daines, S.J., Clark, J.R., Kirkham, A., Strauss, J., Uhlig, C., Lenton, T.M., Valentin, K.,  
704 Pearson, G.A., Moulton, V., Mock, T., 2013. The impact of temperature on marine  
705 phytoplankton resource allocation and metabolism. *Nature Climate Change* 3, 979-984.
- 706 Twitchett, R.J., 2007. The Lilliput effect in the aftermath of the end-Permian extinction event.  
707 *Palaeogeogr. Palaeoclimatol. Palaeoecol.* 252, 132-144.
- 708 U.S. Environmental Protection Agency, 1998. Addendum to "Ambient Water Quality Criteria for  
709 Ammonia--1984.", in: Service, N.T.I. (Ed.), Springfield, VA.
- 710 Van Cappellen, P., Ingall, E.D., 1994. Benthic phosphorus regeneration, net primary production, and  
711 ocean anoxia: A model of the coupled marine biogeochemical cycles of carbon and  
712 phosphorus. *Paleoceanography* 9, 677-692.
- 713 Van Mooy, B.A.S., Keil, R.G., Devol, A.H., 2002. Impact of suboxia on sinking particulate organic  
714 carbon: Enhanced carbon flux and preferential degradation of amino acids via  
715 denitrification. *Geochim. Cosmochim. Acta* 66, 457-465.
- 716 Voight, J.R., Pörtner, H.O., O'Dor, R.K., 1995. A review of ammonia-mediated buoyancy in squids  
717 (cephalopoda: Teuthoidea). *Marine and Freshwater Behaviour and Physiology* 25, 193-  
718 203.
- 719 Wignall, P.B., Bond, D.P.G., Sun, Y., Grasby, S.E., Beauchamp, B., Joachimski, M.M., Blomeier, D.P.G.,  
720 2016. Ultra-shallow-marine anoxia in an Early Triassic shallow-marine clastic ramp  
721 (Spitsbergen) and the suppression of benthic radiation. *Geol. Mag.* 153, 316-331.
- 722 Wignall, P.B., Twitchett, R.J., 2002. Extent, duration, and nature of the Permian-Triassic superanoxic  
723 event. *Geol. Soc. Am. Spec. Paper* 356, 395-413.

724 Winguth, A.M.E., Shields, C.A., Winguth, C., 2015. Transition into a Hothouse World at the Permian–  
725 Triassic boundary—A model study. *Palaeogeogr. Palaeoclimatol. Palaeoecol.* 440, 316-327.

726 Xie, S., Pancost, R.D., Wang, Y., Yang, H., Wignall, P.B., Luo, G., Jia, C., Chen, L., 2010. Cyanobacterial  
727 blooms tied to volcanism during the 5 m.y. Permo-Triassic biotic crisis. *Geology* 38, 447-  
728 450.

729 Zehr, J.P., Ward, B.B., 2002. Nitrogen cycling in the ocean: new perspectives on processes and  
730 paradigms. *Applied and Environmental Microbiology* 68, 1015-1024.

731 Zhang, X., Sigman, D.M., Morel, F.M.M., Kraepiel, A.M.L., 2014. Nitrogen isotope fractionation by  
732 alternative nitrogenases and past ocean anoxia. *Proc. Natl. Acad. Sci. U.S.A.* 111, 4782-  
733 4787.

734 Zhao, L., Chen, Y., Chen, Z.-q., Cao, L., 2013. Uppermost Permian to Lower Triassic Conodont  
735 Zonation from Three Gorges Area, South China. *Palaios* 28, 523-540.  
736

### 737 **Figure and table captions**

738 Fig. 1 The marine nitrogen cycle with sub-models for oxic (A), anoxic (B) and euxinic (C)  
739 conditions. Blue arrows are aerobic reactions; red arrows are anaerobic reactions;  
740 black arrows are reactions with aerobic and anaerobic pathways. Bold lines are  
741 favoured reactions, whereas dashed lines are possible, but unfavoured reactions.  
742 Lightning contributes ~5-8 % of total fixed nitrogen and is generally considered as a  
743 constant input in geological studies. Sub-models represent end-member situations  
744 and do not include the oxygen minimum zone in oxic oceans and oxygenated surface  
745 layers in anoxic and euxinic oceans. In model B, nitrate is consumed by reactions 5, 6,  
746 7 and 8 while resupply of nitrate is inhibited because reaction 4 is a light-inhibited  
747 aerobic reaction. In the model C, nitrogen fixation can be inhibited due to removal of  
748 metabolizable Mo, V and Fe in the water column, leading to suppression of the  
749 nitrogen cycle. Nutrient-N systematically becomes dominated by  $\text{NH}_3/\text{NH}_4^+$  in anoxic  
750 and euxinic conditions. Anammox = anaerobic ammonium oxidation, DNRA =  
751 dissimilatory nitrate reduction to ammonium.

752 Fig. 2 A., Early Triassic palaeogeography, ocean currents and sites of microbial buildups  
753 (Pruss et al., 2006; Chen et al., 2014; Scotese and Moore, 2014). B., Temporal  
754 occurrences of microbial buildups (geographic occurrences shown in A), redox  
755 conditions and equatorial seawater surface-temperatures (Wignall and Twitchett,  
756 2002; Grasby et al., 2012; Sun et al., 2012; Sun et al., 2015) in the Early Triassic. For  
757 redox conditions, the blue colour stands for a globally oxic condition; black stands for  
758 generally anoxic condition while white stands for regional oxic conditions in some  
759 basins. These redox histories derive from studies in Alps, British Columbia, Canadian  
760 Arctic, Japan, South China, Spitsbergen etc. C., Simplified models comparing nitrogen  
761 cycles between a well oxygenated nitrate ocean and an Early Triassic stratified  
762 ammonium ocean. Note that in anoxic oceans denitrification can occur in all water  
763 depths while nutrient-N uptake by phytoplankton can only occur in the euphotic zone.

764 Fig. 3 Cross plots of total nitrogen and total organic carbon content of decarbonatized  
765 sample residues. Intercepts on the TN axis indicate the presence of excess silicate-  
766 bound nitrogen in the samples.

767 Fig. 4 Geochemical records from three study sections, showing a gradual decrease in  $\delta^{15}\text{N}$   
768 in the Early Triassic, a negative shift in  $\delta^{15}\text{N}$  towards the S-S boundary, the covariation  
769 of  $\delta^{13}\text{C}_{\text{carb}}$  and  $\delta^{13}\text{C}_{\text{org}}$  at Jiarong and a near antithetic relationship between  $\delta^{15}\text{N}$  and  
770  $\text{C}/\text{N}_{\text{atomic}}$ . Redox conditions and biostratigraphy from the three sections,  $\delta^{13}\text{C}_{\text{carb}}$  from  
771 Jiarong and  $\delta^{13}\text{C}_{\text{org}}$  from Vindodden are from Zhao et al., (2013), Sun et al. (2015),  
772 Wignall et al. (2016) and Elrick et al. (2017). Redfield ratio ( $\text{C}/\text{N}=6.6$ ) is used as a  
773 reference.

774 Fig. 5 Summary of published  $\delta^{15}\text{N}$  records in the Late Permian to Early Triassic interval,  
775 showing strong denitrification occurred geographically in different settings across the  
776 P-T boundary. The onset and duration of the P-T water column denitrification shows  
777 regional variations, probably controlled by local redox conditions and  
778 palaeoceanographic settings.

779 Fig. 6 Cross plots of V vs. Al, Mo vs. Al, Fe vs. Al and P vs. Al from Jiarong, South China. The  
780 original dataset is fully accessible in Sun et al. (2015).

781 Fig. 7 Depth profile of  $\text{NO}_3^-$ ,  $\text{NH}_4^+$ ,  $\text{O}_2$  and  $\text{S}^{2-}$  concentrations in the highly stratified  
782 contemporary Black Sea, showing a depletion of  $\text{NO}_3^-$  but accumulation of  $\text{NH}_4^+$  in  
783 anoxic water column (modified from Konovalov et al., 2005).

784 Fig. 8 The evolution of the ammonium ocean and changes in energy structures in the  
785 aftermath of the end-Permian mass extinction.

786 Table 1 Comparison of energy yields (standard Gibbs free energy) of aerobic and anaerobic  
787 respiration. Glucose ( $\text{C}_6\text{H}_{12}\text{O}_6$ ) is the most important source of energy for cellular  
788 respiration and thus is used for calculation of comparable energy yields here. Isotopic  
789 enrichment ( $\epsilon$ ) is only for nitrogen reactions and approximated by  $\delta^{15}\text{N}_{\text{product}} -$   
790  $\delta^{15}\text{N}_{\text{reactant}}$  (for  $\epsilon < 1000$  ‰) (McCready et al., 1983; Sigman et al., 2009; Zhang et al.,  
791 2014). Note that DNRA produces less energy than denitrification in term of per mol C;  
792 however, in intense anoxia where nitrate is a limited resource, DNRA yields more  
793 energy than denitrification in measure of per mole N.

794 Table 2 A comparison of  $\delta^{15}\text{N}$  and  $\text{C}/\text{N}_{\text{atomic}}$  ratio in clay-poor rocks and clay-rich rocks that  
795 are closely spaced to each other, showing measured  $\delta^{15}\text{N}$  and  $\text{C}/\text{N}_{\text{atomic}}$  ratios are

796 generally consistent in the two types of rock but C/N<sub>atomic</sub> ratios are more variable in  
797 Early Triassic (TOC poor) rocks.

798 Supplementary materials: Data file [\(including the original dataset and statistical analyses](#)  
799 [on the data\)](#)

800

## Highlights

A conceptual model is established for nitrogen cycle during oceanic anoxic events.

$\delta^{15}\text{N}$  show a decrease in nitrate availability after the end-Permian mass extinction.

The loss of  $\text{NO}_3^-$  was compensated, in anoxic conditions, in the form of  $\text{NH}_4^+$ .

Loss of dissolved nutrient-N in anoxia waters culminated in low ocean productivity.

Ammonium intoxication is a previously unexplored killing mechanism for extinctions.



14 **Abstract:** The aftermath of end-Permian mass extinction was marked by a ~5 million year  
15 interval of poorly-understood, extreme environments that likely hindered biotic recovery.  
16 Contemporary nitrogen isotope variations are considered, using a new conceptual model,  
17 to support a scenario that shows intensive nitrate-removal processes gradually depleted  
18 the global oceanic nitrate inventory during long-lasting oceanic anoxia. Enhanced nitrogen  
19 fixation shifted the oceanic nitrogenous nutrient (nutrient-N) inventory to an ammonium-  
20 dominated state. Ammonium is toxic to animals and higher plants but fertilizes algae and  
21 bacteria. This change in ocean chemistry could account for the intense and unexplained  
22 losses of nektonic taxa and the proliferation of microbial blooms in the Early Triassic. The  
23 transition from a nitrate ocean to an ammonium ocean was accompanied by a decrease in  
24 respiration efficiency of organisms and a shrinking oceanic nutrient-N inventory,  
25 ultimately leading to generally low productivity in the Early Triassic oceans. These  
26 unappreciated nutrient changes during episodes of prolonged ocean anoxia may be the key  
27 life-limiting factor at such times.

28

29 Key words: ocean anoxic event, nitrogen cycle, Early Triassic, ammonium ocean

30

## 31 **1. Introduction**

32           Following the most devastating extinction of the Phanerozoic, the Early Triassic  
33 (~253-247 Ma) interval is considered to have been an extreme hothouse world (Kidder  
34 and Worsley, 2010; Winguth et al., 2015) with equatorial sea-surface temperatures (SSTs)  
35 consistently higher than 32 °C (Sun et al., 2012). Such temperature extremes reduce the  
36 solubility of all gases in the ocean, decrease photosynthetic efficiency in terrestrial plants  
37 and phytoplankton and increase metabolic energy demands (approximately double the  
38 cost for every 10 °C rise according to the  $Q_{10}$  temperature coefficient), and can lead to  
39 intense oceanic anoxia, low biodiversity, and animals with small body sizes (Wignall and  
40 Twitchett, 2002; Twitchett, 2007; Bottjer et al., 2008). The peak of the hothouse occurred  
41 during the Smithian-Spathian (S-S) transition, ~2 million years after the end-Permian mass  
42 extinction, when equatorial SSTs reached ~40 °C (Sun et al., 2012) during a major ~6-8 ‰  
43 negative carbon isotope excursion (Payne et al., 2004; Sun et al., 2015). Many nektonic taxa  
44 that were well adapted to the harsh post-extinction environments finally succumbed at the  
45 S-S transition, suffering even greater proportional losses than at the end of the Permian  
46 (Stanley, 2009).

47           The warm climate and concomitant increased weathering and continental runoff in  
48 the Early Triassic enhanced nutrient delivery to the oceans (Algeo et al., 2011),  
49 theoretically elevating primary productivity and amplifying oxygen deficiency in the water  
50 column (Kump et al., 2005), ultimately producing euxinia with noxious H<sub>2</sub>S. Such  
51 conditions exist today as localized “dead zones” like those found in the Gulf of Mexico  
52 (Rabalais et al., 2002), and they are an oft-cited mechanism for the end-Permian marine  
53 extinction and the delayed Early Triassic recovery (Kump et al., 2005; Algeo et al., 2011).

54 All versions of the death-by-anoxia (euxinia) scenario assume that phosphorus (P) was the  
55 key bio-essential element that controlled productivity levels (Meyer et al., 2008).  
56 Cyanobacterial biomarker spikes and the development of microbialites during and in the  
57 immediate aftermath of the end-Permian crisis (Pruss et al., 2006; Xie et al., 2010)  
58 potentially reflect this high productivity scenario.

59 In addition to P, the other productivity-limiting nutrient in the ocean is N. Unlike P,  
60 nutrient-N availability is not a function of terrestrial input since the oceanic N cycle is  
61 largely internal and biologically-driven (Sigman et al., 2009) (Fig. 1). Under anoxic  
62 conditions denitrification is enhanced and removes nitrate (including nitrite) as N<sub>2</sub> while P  
63 is released from sediments (Van Cappellen and Ingall, 1994). This process, if widespread  
64 and maintained for a prolonged time, generates a nitrate-poor but P-rich ocean (Grasby et  
65 al., 2012; Grasby et al., 2016). The Early Triassic is known for global absence of  
66 phosphorites and other P-rich sedimentary rocks, suggesting intensive P-recycling into  
67 seawater at this time. Although P can be additionally and partially scavenged by Fe  
68 minerals (Feely et al., 1991), Fe shuttles in the Early Triassic oceans were dominated by  
69 pyrite burial, and quantitatively not comparable to banded iron formation deposition in the  
70 Archean and Paleoproterozoic oceans. Thus, P scavenged by Fe minerals is unlikely to have  
71 balanced the excess P input by weathering. Nitrogen could have become the bio-limiting  
72 nutrient in the euphotic zone since marine phytoplankton requires 14-16 times more N  
73 than P (i.e., the Redfield Ratio). The high SSTs of the Early Triassic (Sun et al., 2012) likely  
74 deepened the thermocline, lowered the pole-to-equator temperature gradient and  
75 weakened ocean circulation (Winguth et al., 2015). Under such circumstances, PO<sub>4</sub><sup>3-</sup> and

76  $\text{NO}_3^-$  were probably trapped beneath density barriers, inhibiting nutrient supply to the  
77 euphotic zone (Fig. 2C; Grasby et al., 2016; Penn et al., 2018).

78 To understand the interplay of stratification intensity and the availability of  
79 different nutrients in the Early Triassic oceans, we investigated nitrogen isotope ( $\delta^{15}\text{N}$ )  
80 trends and trace metal concentrations during the Late Permian to Early Triassic in palaeo-  
81 equatorial Tethys (Xiakou and Jiarong sections, South China) and the Boreal Ocean  
82 (Vindodden section, Spitsbergen) (Fig. 2). The results, combined with our new conceptual  
83 model (Fig. 1), suggest the establishment of an “Ammonium Ocean” had severe  
84 consequences for the marine biosphere in the Early Triassic.

85

## 86 **2. Settings**

87 The South China Block was situated at an equatorial position in the eastern Tethys  
88 Ocean in the Early Triassic (Fig. 2A). Palaeogeographically, the study section at Xiakou was  
89 situated on the northern margin of the central Yangtze Platform. The study section at  
90 Jiarong was situated in the centre of the Nanpanjiang Basin, which was a V-shaped, deep  
91 water epicontinental basin that opened south-eastward to the Panthalassa Ocean  
92 (Lehrmann et al., 2003).

93 The Xiakou section (GPS:  $31^\circ 6'55.82''\text{N}$ ,  $110^\circ 48'15.87''\text{E}$ ) is located in Xingshan  
94 County, ~400 km NW of Wuhan. The continuous sequence, from late Changhsingian to  
95 Spathian, crops out alongside a local road. The late Changhsingian strata are characterized  
96 by dark grey to black, marly carbonate and marls. The lithology is replaced upsection by  
97 thinly bedded grey carbonate and shales of the Daye Formation.

98           The Jiarong section (GPS: 25°55'17"N, 106°33'50"E) is located in Huishui County,  
99   ~85 km south of Guiyang City in the Guizhou Province. The Smithian-Spathian succession is  
100 composed of a middle-late Smithian carbonate unit, a latest Smithian black shale unit and  
101 an early Spathian reddish carbonate unit, representing a transition from a basinal setting to  
102 a shallower water environment across the S-S boundary interval (Chen et al., 2015; Sun et  
103 al., 2015). Sediments in the upper part of the Carbonate Unit and the Black Shale Unit are  
104 finely laminated and lack bioturbation. Fossils are generally rare, except for conodonts.  
105 Small ammonoids and scaphopods occur in the Spathian Griotte Unit (Sun et al., 2015).

106           During the Permo-Triassic the Svalbard Archipelago was situated on the  
107 epicontinental shelf of the northern passive margin of Pangaea adjacent to the Boreal  
108 Ocean in high temperate latitudes (~ 55 to 60 °N) (Hounslow et al., 2008). The S-S strata of  
109 central Spitsbergen belong to the Vikinghøgda Formation, and are best documented from  
110 the Vindodden section (Mørk et al., 1999; Wignall et al., 2016).

111           The Vindodden section (GPS: 78°19'39"N, 16°30'19"E) lies in the lower slopes of  
112 Botneheia Mountain, south of Sassenfjorden, a north-eastern arm of Isfjorden. The S-S  
113 sequence consists mainly of a lower unit of dark clay/siltstone unit of Smithian age and an  
114 upper siltstone-sandstone unit of Spathian age. The transition from the Smithian to the  
115 Spathian is marked by a laminated thin dolostone ledge of earliest Spathian age. The  
116 phosphatic black clay/shales atop the Vikinghøgda Formation characterise the Middle  
117 Triassic Botneheia Formation (Wignall et al., 2016). Fossils are rare in the study section,  
118 except for a few *Posidonia* bivalves, *Planolites* trace fossils and ammonoids. Though very  
119 low in abundance, conodonts occur throughout the section, providing biostratigraphic  
120 constraints.

121

### 122 **3. Conceptual Model**

123 Our conceptual model for the oceanic nitrogen cycle consists of four end-members.  
124 They are  $N_2$ , the  $NH_4^+/NH_3$  pair, the  $NO_2^-/NO_3^-$  pair and organic-bonded nitrogen. Amongst  
125 these,  $NH_4^+/NH_3$  and  $NO_2^-/NO_3^-$  are the main forms of dissolved inorganic nutrient-N in the  
126 ocean. The four end-members are linked by eight known reactions in the nitrogen cycle  
127 (Fig. 1). These reactions are further subdivided into aerobic reactions (e.g., nitrification),  
128 anaerobic reactions (e.g., denitrification) and non-redox sensitive reactions (e.g., nitrogen  
129 fixation). This subdivision leads to three simplified sub-models for oceanic nitrogen cycle  
130 in fully oxic (Fig. 1 model A), fully anoxic (Fig. 1 model B) and fully euxinic conditions (Fig.  
131 1 model C). In modern ocean settings, the oceanic nitrogen cycle is dominated by processes  
132 summarized in the model A, while model B describes the nitrogen cycle in the oxygen  
133 minimum zone (OMZ). In warm, stratified and oxygen-depleted Early Triassic oceans, the  
134 models B and C describes the main oceanic nitrogen cycle with the model A only applicable  
135 to the thin, oxygenated surface layer. Though nitrification is an aerobic reaction, it can  
136 occur at very low oxygen concentrations at a lower rate (Bristow et al., 2016). In such  
137 cases, the dissolved nutrient-N inventory is in a subtle balance between nitrate net  
138 production and net consumption, depending on the intensity of ocean anoxia. For example,  
139 at the Black Sea thermocline, anaerobic ammonium oxidation (anammox) bacteria  
140 outcompete aerobic nitrifying bacteria for nitrite (Lam et al., 2007), leading to nitrate and  
141 nitrite net consumption.

142 Nitrate production by nitrification is mainly carried out by ammonia-oxidizing  
143 bacteria (AOB) and ammonia-oxidizing archaea (AOA). This process is generally considered

144 to be light-sensitive for two reasons: 1) some AOB show photoinhibition (e.g., Guerrero and  
145 Jones, 1996), and 2) AOA, though more abundant than AOB in the euphotic zone and not  
146 light-inhibited *per se*, are often outcompeted by phytoplankton for  $\text{NH}_4^+$ . The rate of  
147 nitrification of AOA is lower in the euphotic zone during the day and in the summer due to  
148 limited  $\text{NH}_4^+$  supply while the highest rate occurs at night and in the winter when  
149 competition with phytoplankton is lowest (Smith et al., 2014). Because the euphotic zone is  
150 only a thin layer of water column, the overall rates and efficiency of nitrification in the  
151 ocean depend critically on general redox conditions below the euphotic zone (e.g., Quan  
152 and Falkowski, 2009).

153 Denitrification has a high energy yield (Table 1) and the resupply of nitrate by  
154 nitrification is greatly inhibited in anoxic conditions. Thus, quantitatively nitrate must be in  
155 net consumption in intensive anoxic and euxinic oceans because nitrate produced by  
156 nitrification in the thin, oxygenated surface water column cannot compensate for the  
157 nitrate consumed by denitrification and anammox in anoxic and much thicker deeper  
158 water columns (Fig. 2C). Note that anaerobic ammonium oxidation by manganese oxides  
159 occurs in sediments rather than the water column (e.g., Hulth et al., 1999) and is excluded  
160 here.

161 We use the notion “ammonium ocean” to describe an oceanic state in which  $\text{NO}_2^-$   
162 and  $\text{NO}_3^-$  are largely depleted while  $\text{NH}_4^+$  is the main form of dissolved nutrient-N. Note  
163 that dominance is not necessarily equal to high concentrations. Thus the term “ammonium  
164 ocean” does not necessarily imply *globally* high  $\text{NH}_4^+$  concentrations in the ocean (see 5.3  
165 for further discussion on the heterogeneity of Early Triassic oceans).

166

#### 167 4. Methods (isotope and C/N ratio analyses)

168 For measurements of  $\delta^{13}\text{C}_{\text{org}}$ ,  $\delta^{15}\text{N}$ , and  $\text{C}/\text{N}_{\text{atomic}}$  ratios, weathered surfaces were cut  
169 off the samples. The trimmed samples were washed with distilled water, dried with  
170 compressed air and then milled to fine powder. On average  $\sim 3$  to  $\sim 5$  g powders were  
171 immediately treated with  $\sim 150$  ml 10 % HCl on a hotplate at  $\sim 60$  °C to dissolve any  
172 carbonate. The samples were stirred while slowly adding acid. The decarbonatization  
173 process was generally completed after 48 hours with the complete removal of dolomite and  
174 siderite phases. If not, acid was refreshed and the samples were treated further for 24-48  
175 hours. Insoluble residues were washed repeatedly with deionized water until  $\text{pH} \approx 6$ , dried  
176 in an oven at 60 °C, homogenized using a mortar and stored in small glass containers.

177 The  $\delta^{13}\text{C}_{\text{org}}$  and bulk rock  $\delta^{15}\text{N}$  analyses were performed with a Flash EA 2000  
178 elemental analyser connected online to ThermoFinnigan Delta V Plus mass spectrometer.  
179 All isotope values are reported in the conventional  $\delta$ -notation in per mille (‰) relative to  
180 atmospheric air for  $\delta^{15}\text{N}$  and to V-PDB for  $\delta^{13}\text{C}_{\text{org}}$ . Reproducibility of measurements was  
181 monitored by replicate analyses of laboratory standards (synthetic urea) calibrated to  
182 international standards USGS 40 ( $\delta^{13}\text{C} = -26.39$  ‰;  $\delta^{15}\text{N} = -4.52$  ‰) and USGS 41 ( $\delta^{13}\text{C} =$   
183  $37.63$  ‰;  $\delta^{15}\text{N} = 47.57$  ‰). The reproducibility was  $\pm 0.08$  ‰ ( $2\sigma$ ) for  $\delta^{13}\text{C}_{\text{org}}$ ,  $\pm 0.07$  ‰  
184 ( $2\sigma$ ) for total organic carbon (TOC),  $\pm 0.14$  ‰ ( $2\sigma$ ) for  $\delta^{15}\text{N}$  and  $\pm 0.20$  ‰ ( $2\sigma$ ) for total  
185 nitrogen (TN). The repeatability of samples for  $\delta^{15}\text{N}$  ranges from 0.05 to 0.18 ‰ ( $2\sigma$ ), with  
186 a single case of 0.42 ‰. Note that our  $\delta^{15}\text{N}$  data, as in many other studies in this interval,  
187 represent a  $\delta^{15}\text{N}_{\text{acidified}}$  (rather than  $\delta^{15}\text{N}_{\text{bulk}}$ ) record in a strict sense. The  $\text{C}/\text{N}_{\text{atomic}}$  ratio was  
188 calculated from  $(\text{TOC}/\text{atomic weight of C})/(\text{TN}/\text{atomic weight of N})$ . The TN and TOC  
189 values are positively correlated ( $r^2 = 0.42, 0.68$  and  $0.93$  for Jiarong, Vindodden and Xiakou

190 sections, respectively), suggesting organic matter was the primary source of N (Fig. 3).  
191 Other sources include clay-bound N resulting from diagenetic  $\text{NH}_4^+$  release. The occurrence  
192 of clay-bound N may homogenise, but not necessarily perturb,  $\delta^{15}\text{N}$ .

193 For  $\delta^{13}\text{C}_{\text{carb}}$  analyses, carbonate powders, preferably from micrites, were drilled on  
194 fresh-cut rock surfaces. The powders were reacted with 100 % phosphoric acid at 70 °C in  
195 a Gasbench II connected online with a ThermoFinnigan Delta V Plus mass spectrometer. All  
196 values are reported in per mille relative to V-PDB by assigning  $\delta^{13}\text{C}$  values of +1.95 ‰ to  
197 NBS19 and -47.3 ‰ to IAEA-CO9 and  $\delta^{18}\text{O}$  values of -2.20 ‰ to NBS19 and -23.2 ‰ to  
198 NBS18. Reproducibility was monitored by replicate analysis of laboratory standards  
199 calibrated to NBS 19 and NBS18, and was  $\pm 0.04$  ‰ for  $\delta^{13}\text{C}_{\text{carb}}$  and  $\pm 0.04$  ‰ for  $\delta^{18}\text{O}_{\text{carb}}$   
200 ( $2\sigma$ ;  $n = 20$ ).

201

## 202 **5. Perturbations in global carbon and nitrogen cycles in the Early Triassic**

203 The  $\delta^{13}\text{C}_{\text{carb}}$  values of the Xiakou section show an increase from 1.22 to 2.16 ‰ in  
204 the late Changhsingian. This positive trend is followed by a negative excursion of -2.8 ‰  
205 across the Permian-Triassic (P-T) boundary (at 0 m height). A second,  $\sim -2.0$  ‰ negative  
206 excursion occurs in the mid-late Griesbachian. The largest negative excursion of  $\sim -3.0$  ‰  
207 amplitude occurs in the Smithian.  $\delta^{13}\text{C}_{\text{carb}}$  values decrease from 2.04 to -1.00 ‰ and  
208 remain low in the late Smithian (Fig. 4).

209 The  $\delta^{13}\text{C}_{\text{org}}$  values of Jiarong and Vindodden sections show a similar pattern in the S-  
210 S transition, but differ in absolute values by  $\sim 1$  ‰.  $\delta^{13}\text{C}_{\text{org}}$  from Jiarong shows a positive  
211 excursion of  $\sim 5.5$  ‰ from -31.5 ‰ in the late Smithian to -26.0 ‰ in the earliest Spathian.

212 A slightly smaller positive excursion of  $\sim 4.5$  ‰ is registered at Vindodden, with values  
213 increasing from  $-32.5$  to  $-28.0$  ‰ across the S-S boundary (at 56 m height; Fig. 4).

214 The  $\delta^{13}\text{C}_{\text{carb}}$  and  $\delta^{13}\text{C}_{\text{org}}$  variations from our study sections are consistent with  
215 published  $\delta^{13}\text{C}$  records (Payne et al., 2004; Grasby et al., 2012), and are therefore  
216 considered to record the global signature. The difference in absolute  $\delta^{13}\text{C}_{\text{org}}$  values between  
217 Jiarong and Vindodden is attributed to different primary producers between the equatorial  
218 and Boreal oceans, which were likely to show different carbon isotopic fractionation during  
219 photosynthesis. The  $\delta^{13}\text{C}$  perturbations, redox and sedimentary changes support a scenario  
220 that intense oceanic anoxia in the late Smithian contributed to enhanced burials of organic  
221 carbon (i.e., black shale deposition and positive  $\delta^{13}\text{C}$  excursion) (Sun et al., 2015).

222 The  $\delta^{15}\text{N}$  values from Xiakou record a rapid increase in the late Changhsingian and  
223 reached a  $\sim 3$  ‰ peak immediately above the P-T boundary (Fig. 4). This was followed by a  
224 protracted, gradual decrease from the early Griesbachian to values of  $\sim 0.5$  ‰ in the late  
225 Smithian. At Jiarong,  $\delta^{15}\text{N}$  values match those at Xiakou and then decrease to  $\sim -1$  ‰ across  
226 the S-S boundary (at 24.3 m height); a level that sees the onset of black shale deposition. A  
227 comparable trend across the S-S transition is seen at Vindodden although the  $\delta^{15}\text{N}$  curve is  
228 offset in absolute value by  $\sim 1$  ‰ compared with the other sections (Fig. 4). The  $\text{C}/\text{N}_{\text{atomic}}$   
229 ratio (a measure of organic matter stoichiometry) generally co-varies with, but is opposite  
230 to, the observed trends in  $\delta^{15}\text{N}$ . Thus,  $\text{C}/\text{N}_{\text{atomic}}$  at Xiakou decreases sharply across the P-T  
231 boundary from  $>20$  to  $\sim 2$ , followed by a mild recovery to  $\sim 10$  in the Dienerian and  
232 oscillations around  $\sim 6$  in the Smithian.  $\text{C}/\text{N}_{\text{atomic}}$  at Jiarong increases steadily from  $\sim 10$  to  
233  $\sim 30$  towards the S-S boundary, followed by a decrease above its maxima of  $\sim 40$  in the

234 earliest Spathian. At Vindodden,  $C/N_{\text{atomic}}$  increases from  $\sim 11$  to  $\sim 20$  towards the S-S  
235 boundary (at 56 m height) before decreasing to  $\sim 15$  in the early Spathian.

236 The  $\delta^{15}\text{N}$  data show minor regional variations compared to published records, with  
237 differences occurring mainly in the Late Permian (Fig. 5). Water column denitrification  
238 occurred near the P-T boundary at Xiakou whereas in Arctic Canada and western Alberta  
239 denitrification prevailed in the latest Permian. The  $\delta^{15}\text{N}$  shifts seen in the Early Triassic at  
240 Xiakou and Jiarong are comparable to reported patterns from the Sverdrup Basin (Knies et  
241 al., 2013; Grasby et al., 2016) and the western margin of Pangaea (Schoepfer et al., 2012).  
242 Since South China, the Sverdrup Basin and western Alberta were situated in very different  
243 climatic and oceanographic settings, and yet were connected to the Panthalassa ocean, we  
244 interpret their comparable  $\delta^{15}\text{N}$  variations in the Early Triassic to reflect the global ocean  
245 signatures (Fig. 5). The divergence in  $\delta^{15}\text{N}$  between Vindodden and other regions probably  
246 reflects a minor nitrate input from a polar current to Spitsbergen as well as its slightly  
247 more restricted environment (Fig. 2A).

248

## 249 **6. Discussion**

### 250 *6.1 Influence of diagenesis on $\delta^{15}\text{N}$ and $C/N_{\text{atomic}}$ ratio*

251 Diagenesis can potentially alter both sedimentary  $\delta^{15}\text{N}$  and the  $C/N_{\text{atomic}}$  ratio. For  
252 example, degradation of amino acid during early diagenesis releases  $\text{NH}_4^+$  to pore water. If  
253 the  $\text{NH}_4^+$  is absorbed by clay minerals, then sedimentary  $\delta^{15}\text{N}$  would show minor changes  
254 compared to the original signature. Positive intercepts on the TN axis in our TN-TOC cross  
255 plot (Fig. 3) indicate the presence of excess clay-bound nitrogen in our samples. We  
256 consider our  $\delta^{15}\text{N}$  to a be a faithfully record because data measured from adjacent

257 carbonate and marl (shale) samples, although with large variations in TOC and clay  
258 content, show consistent values in  $\delta^{15}\text{N}$  (Table 2) and our sections are from different  
259 sedimentary basins and underwent different diagenetic and burial history, and yet the  $\delta^{15}\text{N}$   
260 records are largely comparable with each other and published records. Only, the onset and  
261 duration of P-T water column denitrification show regional variations (Fig. 5). On the other  
262 hand, diagenesis can significantly alter the  $\text{C}/\text{N}_{\text{atomic}}$  ratio, especially in TOC-poor, clay-rich  
263 sediments, and cause divergence from the Redfield Ratio to higher values. Diagenetic  
264 sulphate reduction, which removes C but not N, can lower  $\text{C}/\text{N}_{\text{atomic}}$  ratio.

## 265 *6.2 Intensified denitrification, low sulphate concentration and a nitrate starved ocean*

266 The oceanic N cycle is largely microbially mediated (Altabet, 2006). The onset of  
267 intense and widespread anoxia in the latest Permian saw a profound change in dominance  
268 amongst oceanic microbial communities from aerobic to anaerobic respiration. Since the  
269 energy yield from denitrification ( $\Delta G^0 = -445 \text{ kJ/mol C}$ )<sup>1</sup> is almost as efficient as that of  
270 aerobic respiration ( $\Delta G^0 = -478 \text{ kJ/mol C}$ ), nitrate is the first energy source to be consumed  
271 in anoxic environments (Table 1). Thus, the shift to microbial anaerobic respiration is  
272 manifest as the positive  $\delta^{15}\text{N}$  trend seen in the late Changhsingian at Xiakou and elsewhere  
273 (Fig. 5). This indicates widespread water column denitrification, and coincides with the  
274 onset of intensive anoxia (e.g., Grasby et al., 2012; Elrick et al., 2017).

275 Despite some regional variations,  $\delta^{15}\text{N}$  records from different settings all indicate  
276 strong denitrification occurring across the P-T boundary, followed by a dominance of

---

<sup>1</sup>  $\Delta G^0$  represents the standard Gibbs free energy of formation, a thermodynamic measure of energy absorption or yield of a reaction at the standard conditions (25 °C and 100 kPa). Positive values suggest a reaction absorbs energy while negative values suggest a reaction yield energy. The more negative the values, the more energy is yielded through the reaction.

277 nitrogen fixation in the Early Triassic (Fig. 5). The  $\delta^{15}\text{N}$  values in the Early Triassic of our  
278 study sections are depleted in  $^{15}\text{N}$  compared to the average  $\delta^{15}\text{N}$  of modern oceans ( $\sim 5$   
279 ‰)(Altabet, 2007). Nitrate was likely depleted and nitrogen fixation dominated in both  
280 northern Boreal and equatorial Tethyan waters at this time. Reducing conditions amplify  
281 anaerobic reactions such as denitrification and anammox; reactions that selectively  
282 consume nitrate depleted in  $^{15}\text{N}$  ( $\epsilon = 5\text{--}30$  ‰) and produce non-nutritious  $\text{N}_2$ . As nitrate  
283 consumption continues,  $^{15}\text{N}$  becomes enriched in seawater, resulting in heavy  $\delta^{15}\text{N}$  values  
284 in sedimentary organic matter (e.g.  $\delta^{15}\text{N} > 5$  ‰). In modern oceans, intensive  
285 denitrification occurs in the oxygen minimum zone where organic matter and nitrate are  
286 both replete (Fig. 2C). In the Early Triassic anoxic oceans, denitrification and anammox  
287 probably occurred over a broad range of depths and theoretically would have generated  
288 high sedimentary  $\delta^{15}\text{N}$  values (e.g.  $\delta^{15}\text{N} = \sim 5\text{--}15$  ‰). Instead,  $\delta^{15}\text{N}$  values from both  
289 equatorial and boreal settings are in the  $-1$  to  $2$  ‰ range. This can be explained through a  
290 nitrate-starved scenario in which the isotopic fractionation effect of denitrification and  
291 anammox decreases due to very low nitrate availability (i.e., exceptionally high  
292 denitrification rate) and intense seawater stratification while nitrogen fixation is the only  
293 source of nutrient-N. Alternatively, low  $\delta^{15}\text{N}$  could suggest nitrate levels become so low  
294 that the heavy  $\delta^{15}\text{N}$  of the residual nitrate can no longer dominate the isotopic composition  
295 of biomass. As the thermocline deepened during the Early Triassic hothouse, nitrate supply  
296 from deep-water environments to the euphotic zone had to overcome the density barrier,  
297 and this could only be achieved by diffusion (Fig. 2C). Diffusion would eventually have  
298 drained the nitrate inventory of deep-water reservoirs. In open water settings, nitrate  
299 consumption exceeding nitrate production was probably a protracted process, controlled

300 by the evolution and intensity of ocean anoxia. This is consistent with the observed  
301 prolonged and gradual  $\delta^{15}\text{N}$  decrease from the earliest Triassic to the S-S boundary (Grasby  
302 et al., 2016). Localized depletion of nitrate on some isolated platforms, marked by  $\delta^{15}\text{N}$   
303 falling to  $\sim 0$  ‰, occurred much earlier at the P-T boundary (Fig. 5); this was probably due  
304 to a lack of nitrate resupply from the deep reservoirs in such settings.

305         The near-antithetic relationship between  $\delta^{15}\text{N}$  and the  $\text{C}/\text{N}_{\text{atomic}}$  ratio at the S-S  
306 transition suggests that a common cause simultaneously drove  $\delta^{15}\text{N}$  to lower values and  
307 the  $\text{C}/\text{N}_{\text{atomic}}$  ratio to higher values (and vice versa). This is unlikely to be due to the input of  
308 terrestrial organic matter (which typically has low  $\delta^{15}\text{N}$  and high  $\text{C}/\text{N}_{\text{atomic}}$  ratios) because,  
309 with the near-extinction of land plants at the end of the Permian and the subsequent low  
310 terrestrial biomass on Pangea (Looy et al., 1999), terrestrial N input is unlikely to have  
311 affected the isotopic composition of the oceanic N pool. Instead, the factor that drove the  
312  $\delta^{15}\text{N}$  and  $\text{C}/\text{N}_{\text{atomic}}$  ratio in opposite directions was probably the bioavailability of nitrate. In  
313 the case of low nitrate availability and long-term anoxia, nitrate-removal processes utilize  
314 nitrate and the corresponding isotopic fractionation effects decrease while nitrogen  
315 fixation is enhanced thereby compensating for the nutrient-N loss. Both processes lower  
316  $\delta^{15}\text{N}$  values of organic N. At the same time, anoxia enhances bacterial recycling of N-rich  
317 amino acids from organic matter (Van Mooy et al., 2002), leading to a more intense loss of  
318 sedimentary N during diagenesis and higher  $\text{C}/\text{N}_{\text{atomic}}$  ratios.

319         Low sulphate concentrations and episodic euphotic zone euxinia characterize the  
320 Early Triassic oceans (Grice et al., 2005; Song et al., 2014). These are largely, or at least  
321 partially, due to enhanced bacterial sulphate reduction, perhaps due to high marine  
322 productivity (Schobben et al., 2015). However, with increasing water column  $\text{O}_2$  deficiency,

323 heterotrophic bacteria favour energy extraction pathways with high yields. Sulphate  
324 reduction ranks low in this respect amongst anaerobic respiration (Table 1) and is only  
325 favoured once nitrate is depleted (Altabet, 2006). We thus argue that enhanced sulphate  
326 reduction in the Early Triassic oceans was probably a response to a functional shift in  
327 microbial communities from nitrate consuming ( $\Delta G^0 = -445$  kJ/mol C) to sulphate  
328 consuming ( $\Delta G^0 = -61$  kJ/mol C) and thus did not necessarily require eutrophication  
329 (Schobben et al., 2016).

### 330 *6.3 Enhanced nitrogen fixation, Mo limitation and a shift in nutrient-N inventory*

331 The protracted anoxic conditions in the Early Triassic promoted nitrogen fixation.  
332 The  $\delta^{15}\text{N}$  values of  $\sim 0.5$  to  $-1$  ‰ at Jiarong and Xiakou suggest  $\text{N}_2$  fixation dominated  
333 equatorial oceans. A similar scenario is suggested for Cretaceous oceanic anoxic events  
334 when comparably low  $\delta^{15}\text{N}$  values are associated with black shale deposition (Junium and  
335 Arthur, 2007), highlighting a key role of diazotrophs (nitrogen fixers) under anoxic  
336 conditions.

337 Biological nitrogen fixation is an enzyme-catalyzed  $\text{N}_2$  reduction, which has low  
338 energy yields ( $\Delta G^0 = -157$  kJ/mol N) and has to overcome a large kinetic barrier to break  
339 three N-N bonds in the  $\text{N}_2$  molecule (Altabet, 2006). This can only be achieved by  
340 diazotrophs that are exclusively prokaryotes. Most diazotrophs are anaerobic bacteria or  
341 archaea except for diazotrophic cyanobacteria which have special cell walls that inhibit  
342 oxygen diffusion (Altabet, 2006). This is because the nitrogenase enzyme has a metal  
343 center consisting of either Mo-Fe, V-Fe or Fe-only complexes and its function is irreversibly  
344 inhibited by free oxygen (Berman-Frank et al., 2003). Thus, diazotrophs generally prefer  
345 anoxic environments, require P as a nutrient, and metal ions for synthesizing the

346 nitrogenase enzyme. Phosphorus availability may not have been a limiting factor in the  
347 Early Triassic ocean because of 1) increased terrestrial P input via enhanced weathering; 2)  
348 recycling of P from anoxic sediments; and 3) reduced metazoan uptake following  
349 extinctions of shelly fossils that incorporated P in CaCO<sub>3</sub> shells and biogenic apatite. This  
350 inference is supported by data from Jiarong, where P and Al contents are positively  
351 correlated ( $r = 0.77, p < 0.05$ ) but not as significantly as Fe vs. Al ( $r = 0.96, p < 0.05$ ) and V  
352 vs. Al ( $r = 0.95, p < 0.05$ ) (Fig. 6), suggesting P sources were not entirely terrestrial.

353         Metabolizable trace metals Mo(VI), V(V) and Fe(II) are redox-sensitive and they can  
354 be scavenged from the water column into sediments under intensely anoxic and euxinic  
355 conditions. A scarcity of such trace nutrients could severely suppress nitrogen fixation,  
356 leading to a pause in nitrogen cycling after nitrate depletion and a consequent collapse in  
357 oceanic productivity (Fig. 1, model C). However, such a scenario seemingly did not occur, at  
358 least not globally or for the long term, in the Early Triassic. This is probably because Fe(II)  
359 availability was sufficiently high, being reduced from Fe oxides from riverine input and  
360 aeolian dust or directly derived from hydrothermal activity at mid-ocean ridges. High Fe(II)  
361 availability is consistent with the development of ferruginous conditions (Clarkson et al.,  
362 2016) and the global abundance of pyrite framboids in Early Triassic sediments (Wignall  
363 and Twitchett, 2002).

364         In contrast, the Mo reservoir was probably much smaller than the Fe reservoir with  
365 minor input into large sinks, and could be depleted more easily. However, Mo availability  
366 cannot be easily evaluated because Mo tends to sink in sediments under anoxic-euxinic  
367 conditions. Thus Mo concentration measured from sedimentary rocks mainly reflects water  
368 column redox changes and does not necessarily mirror Mo availability in seawater. A

369 proper estimation would require multiple speculations on Mo input and sink. Mo limitation  
370 in this case is inferred from indirect evidence from  $\delta^{15}\text{N}$ . Mo-Fe nitrogenase is much more  
371 efficient than V-Fe and Fe-only nitrogenase (Berman-Frank et al., 2003). A shift in  
372 nitrogenase type leads to a change in the isotopic fractionation during nitrogen fixation  
373 ( $^{14}\text{N}$  is preferably used) which could have resulted in more negative values in sedimentary  
374  $\delta^{15}\text{N}$  (Zhang et al., 2014). The sporadic development of more negative  $\delta^{15}\text{N}$  values ( $< -2 \text{ ‰}$ )  
375 in the Jiarong section might have been a manifestation of short pulses of Mo limitation.  
376 Alternatively, (or collectively), these low  $\delta^{15}\text{N}$  values may also be explained by partial  $\text{NH}_4^+$   
377 uptake. Low  $\delta^{15}\text{N}$  values are comparably rare throughout Earth's history, including the  
378 Precambrian, where Mo was likely much less abundant than at any time in the Phanerozoic  
379 (Stüeken et al., 2016). However,  $\delta^{15}\text{N}$  values  $< -2 \text{ ‰}$  are seen during intensive anoxia, such  
380 as during the oceanic anoxic events in the early Jurassic and middle Cretaceous (Jenkyns et  
381 al., 2001; Junium and Arthur, 2007), suggesting Mo limitation and/or  $\text{NH}_4^+$ -rich conditions  
382 may have occurred more frequently than previously thought.

383 Nitrate (including nitrite) and ammonium (including ammonia) are two end  
384 members of oceanic nutrient-N (Fig. 1). In oxic waters, nitrification actively converts  $\text{NH}_4^+$   
385 to  $\text{NO}_3^-$ . Many primary producers rely on the nitrate supply from deep waters, brought up  
386 by mixing and upwelling (Fig. 2C). In contrast, in anoxic oceans, anammox, denitrification  
387 and dissimilatory nitrate reduction to ammonium (DNRA) compete for nitrate for high  
388 anaerobic energy yields (Fig.1; Table 1). Anammox consumes both  $\text{NH}_4^+$  and  $\text{NO}_2^-$  and  
389 produces non-nutritious  $\text{N}_2$ . In the case of intense anoxia (e.g., fast expansion of OMZ) and  
390 especially euxinia, DNRA produces an electron sink and thus outcompetes denitrification  
391 for nitrate (An and Gardner, 2002; Giblin et al., 2013) (Table 1). Such conditions, typically

392 accompanied by high temperatures, high organic carbon burial and sulphate reduction  
393 rates, are seen in polluted coastal environments today but were likely widespread in the  
394 Early Triassic oceans, especially during the P-T transition and in the late Smithian (Grasby  
395 et al., 2012; Sun et al., 2012; Schobben et al., 2015; Sun et al., 2015). Unlike denitrification  
396 and anammox, DNRA recycles nitrate to bioavailable  $\text{NH}_4^+$ . A combination of nitrate net  
397 consumption and enhanced nitrogen fixation and DNRA likely led to a shift from a  $\text{NO}_3^-$   
398 dominated nutrient-N inventory to one dominated by  $\text{NH}_4^+$  (Fig. 1, models B and C; Fig. 8).  
399 Though  $\text{NH}_4^+$  dominance does not necessarily result in  $\text{NH}_4^+$  accumulation to high  
400 concentrations. Once established, the only pathway to reverse this shift is through  
401 nitrification, which is a light-sensitive aerobic reaction (Zehr and Ward, 2002), thus  
402 requiring oxygenation of deeper (dark) waters.

#### 403 *6.4 Comparison with the modern Black Sea and the heterogeneity of Early Triassic oceans*

404 The Black Sea is the world's largest anoxic basin and a contemporary analogue for  
405 an ammonium ocean that can be used to test our conceptual model. The  $\text{NH}_4^+$   
406 concentration in the Black Sea is  $\sim 0 \mu\text{M}$  in oxygenated surface waters but increases  
407 significantly with depth and oxygen deficiency to  $\sim 30 \mu\text{M}$  at 250 m depth while nitrate  
408 concentration remains  $\sim 0 \mu\text{M}$  below the suboxic-anoxic interface (Fig. 7; Kuypers et al.,  
409 2003). Our model fits these observations— nitrate is depleted while ammonium  
410 accumulates in anoxic environments (Fig. 1 model B).

411 Accumulation of  $\text{NH}_4^+$  in the Black Sea is at least partially due to strong stratification  
412 of the water column (Fig. 7). The freshwater discharge from the Danube and other rivers  
413 creates an oxic cap that prevents water column mixing. Though not a perfect analogue, the  
414 P-T oceans are also generally considered to be highly stratified due to extreme hothouse

415 climate and stagnation of ocean circulations (e.g., Hotinski et al., 2001; Winguth et al.,  
416 2015).

417 In contrast to Black Sea surface waters, where nitrate still exists, low latitude  
418 shallow-water Early Triassic  $\delta^{15}\text{N}$  values fall to  $\sim 0$  ‰ and lower immediately above the P-  
419 T boundary (Luo et al., 2011) and at the S-S transition, which suggests the nutrient-N  
420 supply to surface waters was composed entirely of newly fixed-N. This was probably due to  
421 intense photic zone euxinia (Grice et al., 2005; Cao et al., 2009) which inhibited nitrification  
422 in the surface water. In contrast,  $\delta^{15}\text{N}$  values from northern higher latitudes (e.g.,  
423 Vindodden) have a mixed signature of N-fixation and nitrate. The presence of nitrate  
424 suggests nitrification was still partially active in these settings at night, in the winter  
425 and/or in the oxygenated lower euphotic zone.

#### 426 *6.5 Ammonium fertilization*

427 Marine phytoplankton and newly generated organic matter have a near-constant  
428 stoichiometric composition ratio — C:N:P = 106:16:1, known as the Redfield ratio. The  
429 Redfield stoichiometry suggests a higher demand for nutrient-N than P amongst primary  
430 producers. At higher temperatures, eukaryotic phytoplankton have a reduced demand for P  
431 required for cellular protein synthesis and shifts the oceanic nutrient structure to one that  
432 is N-limited (Toseland et al., 2013). Diazotrophic cyanobacteria are uniquely suited to such  
433 environments due to their self-sufficiency in nutrient-N. The recycling of cyanobacterial  
434 biomass occurs rapidly during heterotrophy in the euphotic zone, releasing  $\text{NH}_4^+$  that can  
435 be assimilated by other phytoplankton (Fulton et al., 2012). Such processes could continue  
436 to the point that P is consumed in the euphotic zone and then becomes the limiting  
437 nutrient. Given this constraint and the lack of major shifts in the Redfield N/P ratio in the

438 Early Triassic (Grasby et al., 2016), the size of the ancient deep ocean  $\text{NH}_4^+$  reservoir could  
439 not have been much greater than the modern ocean nitrate reservoir. This suggests an  
440 Early Triassic deep ocean  $\text{NH}_4^+$  concentration was unlikely to have been greater than  $\sim 50$   
441  $\mu\text{M}$ .

442         Phytoplankton (both eukaryotes and cyanobacteria) generally prefer  $\text{NH}_4^+$  to  $\text{NO}_3^-$  as  
443 a nutrient source, because of the redundant energy costs expended when reducing  $\text{NO}_3^-$  to  
444  $\text{NH}_4^+$  (Zehr and Ward, 2002). The exception is diatoms which generally prefer  $\text{NO}_3^-$  as a  
445 nutrient-N source but they only appeared in the Jurassic. One contemporary example for  
446  $\text{NH}_4^+$  fertilization is the long-lasting Texas Brown Tide at the Laguna Madre/Baffin Bay  
447 estuary, caused by the alga *Aureomonas lagunensis*. This species is able to use  $\text{NH}_4^+$  or  $\text{NO}_2^-$   
448 but not  $\text{NO}_3^-$  and its enduring bloom was fertilized by  $\text{NH}_4^+$  produced by DNRA in an  
449 environment with high sulphide concentrations (An and Gardner, 2002). Similarly, regional  
450 primary productivity increase and stromatolite development (e.g., Pruss et al., 2006; Chen  
451 et al., 2014) in the Early Triassic were likely stimulated by  $\text{NH}_4^+$  fertilization. The extensive  
452 microbialite build-ups in the aftermath of end-Permian mass extinction (Fig. 2A, B) were  
453 probably constructed by diazotrophs ( $\text{NH}_4^+$  self-sufficient by N-fixation), or otherwise  
454 fertilized by ambient  $\text{NH}_4^+$ . The onset of microbialite development in the earliest  
455 Griesbachian clearly coincided with enhanced nitrogen fixation (Cao et al., 2009; Xie et al.,  
456 2010; Luo et al., 2011) — a feature also seen during the S-S transition. The bloom of  
457 prasinophyte algae immediately after the end-Permian mass extinction while N-fixation by  
458 cyanobacteria was occurring, is suggested to have provided prasinophytes with  $\text{NH}_4^+$  in  
459 nutrient-limited environments (Jia et al., 2012). The demise of microbialites towards the  
460 Middle Triassic (Fig. 2B) was likely due to a general amelioration of environmental stresses

461 and the re-establishment of potent nitrification, reducing  $\text{NH}_4^+$  during deep-water re-  
462 oxygenation (Fig. 1, model A).

### 463 *6.6 Ammonium intoxication*

464         Although it fertilizes phytoplankton,  $\text{NH}_4^+$  is a major metabolic waste and can be  
465 lethal to both animals and higher plants at high concentrations (Britto and Kronzucker,  
466 2002).  $\text{NH}_4^+$  accumulation, for instance, is a widespread problem in modern fish farming.  
467 Terrestrial animals and birds convert  $\text{NH}_4^+$  to the much less toxic urea but aquatic animals  
468 generally rely on direct excretion of  $\text{NH}_4^+$  to ambient water (Ip et al., 2001). The lethal  
469 concentration of ammonium for a wide range of marine vertebrates is  $12.5 \mu\text{M}$  (Knoph and  
470 Thorud, 1996; U.S. Environmental Protection Agency, 1998), much lower than the  $\sim 50 \mu\text{M}$   
471 maximum estimated for the Early Triassic oceans. In general, invertebrates are more  
472 tolerant to ammonia (i.e., total ammonia =  $\text{NH}_4^+$  and  $\text{NH}_3$ ) than vertebrates while  
473 freshwater animals are more tolerant than marine animals. The toxicity of total ammonia  
474 manifests as damage to the central nervous system in vertebrates and is amplified at higher  
475 pH (e.g., in seawater). This is because  $\text{NH}_4^+$  is more toxic but less diffusive while most  
476 animal membranes are more permeable to  $\text{NH}_3$  (Ip et al., 2001). Remineralization of  
477 organic N in anoxic environments exclusively leads to  $\text{NH}_4^+$  and  $\text{NH}_3$  accumulation (Fig. 1,  
478 models B and C). Since protein decay is independent of redox conditions, and nitrification is  
479 inhibited in anoxic waters, degradation of organic remains and diazotrophs could have, at  
480 least in short term, produced excessive  $\text{NH}_4^+$  that may, at least in part, explain the hitherto  
481 enigmatic Early Triassic extinction/changeover events amongst nekton such as conodonts  
482 and fish. Such groups would be somewhat immune to the typical end-Permian scenario of  
483 high temperatures and low oxygen levels due to their ability to migrate to higher latitudes

484 and their upper water column habitats. Neither factor would help nekton escape  $\text{NH}_4^+$ - $\text{NH}_3$   
485 poisoning. Even at modest increases in concentrations, the swimming ability of animals  
486 such as fish is impaired (Ip et al., 2001).

487 On the other hand, cephalopods are exclusively carnivores with fast growth rates for  
488 most of their life cycle. They have a high demand for proteins and the dominance of amino  
489 acid metabolism leads to a high  $\text{NH}_4^+$  accumulation in their systems (Lee, 1995). Some  
490 groups of cephalopods have much high tolerance of  $\text{NH}_4^+$  because they retain this  
491 metabolic waste in their tissues to achieve neutral buoyancy while other groups did not  
492 develop this physiological mechanism, but instead transform toxic  $\text{NH}_4^+$  to  $\text{N}_2$  gas (e.g.,  
493 *Nautilus*) or develop jelly-like chloride compounds to maintain buoyancy (Voight et al.  
494 1995). Thus, the fast turnover of ammonoids during the end-Permian mass extinction may  
495 reflect the success of those groups with a tolerance for high  $\text{NH}_4^+$  concentrations.  $\text{NH}_4^+$   
496 levels in ammonoid soft tissue were probably often high and the post mortem release  
497 during burial maintains high ambient pH levels thus inhibiting calcium phosphate  
498 replacement (Clements et al., 2017). This likely explains why ammonoid soft body tissue is  
499 rarely seen in fossil Lagerstätte.

500 Ammonium concentrations are not recorded in sedimentary rocks. Quantitative  
501 Earth system modelling studies are needed to better constrain the concentration of total  
502 ammonia in the P-T oceans and to further validate this hypothesis. If correct, ammonium  
503 poisoning is a previously unidentified end-Permian and Early Triassic killing mechanism  
504 (Fig. 8) and, once accumulated, its removal from seawater is difficult under anoxic and  
505 stratified oceanic conditions.

506 *6.8 Loss of dissolved nutrient-N in anoxic waters*

507           Since nitrification can occur at low oxygen concentrations, establishment of  
508 ammonium oceans in the Phanerozoic could only occur in highly stratified oceans and  
509 during intensive ocean anoxic events. In cases of moderately anoxic conditions or fast  
510 oscillations in (dys)oxic and anoxic conditions, ammonium is likely converted to nitrate,  
511 which would then be denitrified. Additionally, as observed in OMZs in contemporary Omani  
512 Shelf, offshore Peru and elsewhere, DNRA and anammox bacteria can form DNRA-  
513 Anammox coupling and account for nutrient-N losses in areas of no detectable  
514 denitrification (Jensen et al., 2011). These processes could result in losses of both  
515 ammonium and nitrate, leading to a decrease in dissolved inorganic nutrient-N inventory  
516 (Fig. 8).

517

## 518 **7. Conclusion**

519           Assertions that primary productivity in the Early Triassic oceans was either  
520 universally high or universally low are both untenable. The transition from nitrate oceans  
521 to ammonium oceans was accompanied by decreases in both the respiration efficiency of  
522 organisms and in the oceanic nutrient-N reservoir (Fig. 8). Though controlled by regional  
523 redox and oceanographic setting,  $\text{NH}_4^+$  could temporarily and regionally boost primary  
524 productivity although it was probably low in general since most nutrient-N was likely lost  
525 during persistent periods of anoxia. Enhanced sulphate reduction, which is widely implied  
526 in the P-T oceans, could be attributed to a functional shift in microbial communities from  
527 nitrate consumption to sulphate consumption in a nitrate-starved ocean and thus does not  
528 necessarily require eutrophication.

529 Ammonium intoxication is one of the worst case scenarios of ammonium ocean  
530 which, in turn, is likely a synergetic effect of widespread ocean anoxia and intensive water  
531 column stratification. Though remaining conceptual and awaiting Earth system modelling  
532 studies to further constrain, ammonia toxicity has not been considered in geological  
533 studies, and yet it may have played a substantial role in suppressing complex life before the  
534 rise of oxygen and probably in selectivity during many past extinctions.

535  
536 **Acknowledgments:** This is a contribution to DFG (German Science Foundation) Research  
537 Unit TERSANE (FOR 2332: Temperature-related stressors as a unifying principle in ancient  
538 extinctions; Project Jo 219/15). National Natural Science Foundation of China (41821001,  
539 41602026, 41602016), the National Key R&D Program of China (2016YFA0601104), and  
540 Natural Environment Research Council of UK (RG.EVEA.109961; NE/J01799X/1)  
541 financially supported this study. Editor T. Mather is thanked for professional handling.  
542 Constructive comments from E. Stüeken and two anonymous reviewers improved this  
543 paper. K. De Baets and C. Scotese are thanked for fruitful discussions.

544  
545 **References**

546 Algeo, T.J., Chen, Z.Q., Fraiser, M.L., Twitchett, R.J., 2011. Terrestrial–marine teleconnections in the  
547 collapse and rebuilding of Early Triassic marine ecosystems. *Palaeogeogr. Palaeoclimatol.*  
548 *Palaeoecol.* 308, 1-11.

549 Altabet, M.A., 2006. Isotopic tracers of the marine nitrogen cycle: Present and past, in: Volkman, J.K.  
550 (Ed.), *Marine Organic Matter: Biomarkers, Isotopes and DNA*. Springer Berlin Heidelberg,  
551 Berlin, Heidelberg, pp. 251-293.

552 Altabet, M.A., 2007. Constraints on oceanic N balance/imbalance from sedimentary <sup>15</sup>N records.  
553 *Biogeosciences* 4, 75-86.

554 An, S., Gardner, W.S., 2002. Dissimilatory nitrate reduction to ammonium (DNRA) as a nitrogen link,  
555 versus denitrification as a sink in a shallow estuary (Laguna Madre/Baffin Bay, Texas).  
556 *Marine Ecology Progress Series* 237, 41-50.

- 557 Berman-Frank, I., Lundgren, P., Falkowski, P., 2003. Nitrogen fixation and photosynthetic oxygen  
558 evolution in cyanobacteria. *Research in Microbiology* 154, 157-164.
- 559 Bottjer, D.J., Clapham, M.E., Fraiser, M.L., Powers, C.M., 2008. Understanding mechanisms for the  
560 end-Permian mass extinction and the protracted Early Triassic aftermath and recovery.  
561 *GSA Today* 18, 4-10.
- 562 Bristow, L.A., Dalsgaard, T., Tiano, L., Mills, D.B., Bertagnolli, A.D., Wright, J.J., Hallam, S.J., Ulloa, O.,  
563 Canfield, D.E., Revsbech, N.P., Thamdrup, B., 2016. Ammonium and nitrite oxidation at  
564 nanomolar oxygen concentrations in oxygen minimum zone waters. *Proc Natl Acad Sci U S*  
565 *A* 113, 10601-10606.
- 566 Britto, D.T., Kronzucker, H.J., 2002.  $\text{NH}_4^+$  toxicity in higher plants: a critical review. *Journal of Plant*  
567 *Physiology* 159, 567-584.
- 568 Cao, C., Love, G.D., Hays, L.E., Wang, W., Shen, S., Summons, R.E., 2009. Biogeochemical evidence for  
569 euxinic oceans and ecological disturbance presaging the end-Permian mass extinction  
570 event. *Earth Planet. Sci. Lett.* 281, 188-201.
- 571 Chen, Y., Jiang, H., Lai, X., Yan, C., Richoz, S., Liu, X., Wang, L., 2015. Early Triassic conodonts of  
572 Jiarong, Nanpanjiang Basin, southern Guizhou Province, South China. *J. Asian Earth Sci.*  
573 105, 104-121.
- 574 Chen, Z.-Q., Wang, Y., Kershaw, S., Luo, M., Yang, H., Zhao, L., Feng, Y., Chen, J., Yang, L., Zhang, L.,  
575 2014. Early Triassic stromatolites in a siliciclastic nearshore setting in northern Perth  
576 Basin, Western Australia: Geobiologic features and implications for post-extinction  
577 microbial proliferation. *Global Planet. Change* 121, 89-100.
- 578 Clarkson, M.O., Wood, R.A., Poulton, S.W., Richoz, S., Newton, R.J., Kasemann, S.A., Bowyer, F.,  
579 Krystyn, L., 2016. Dynamic anoxic ferruginous conditions during the end-Permian mass  
580 extinction and recovery. *Nature Communications* 7, 12236.
- 581 Clements, T., Colleary, C., De Baets, K., Vinther, J., 2017. Buoyancy mechanisms limit preservation of  
582 coleoid cephalopod soft tissues in Mesozoic Lagerstätten. *Palaeontology* 60, 1-14.
- 583 Elrick, M., Polyak, V., Algeo, T.J., Romaniello, S., Asmerom, Y., Herrmann, A.D., Anbar, A.D., Zhao, L.,  
584 Chen, Z.-Q., 2017. Global-ocean redox variation during the middle-late Permian through  
585 Early Triassic based on uranium isotope and Th/U trends of marine carbonates. *Geology*  
586 45, 163-166.
- 587 Feely, R.A., Trefry, J.H., Massoth, G.J., Metz, S., 1991. A comparison of the scavenging of phosphorus  
588 and arsenic from seawater by hydrothermal iron oxyhydroxides in the Atlantic and Pacific  
589 Oceans. *Deep Sea Research Part A. Oceanographic Research Papers* 38, 617-623.
- 590 Fulton, J.M., Arthur, M.A., Freeman, K.H., 2012. Black Sea nitrogen cycling and the preservation of  
591 phytoplankton  $\delta^{15}\text{N}$  signals during the Holocene. *Global Biogeochem. Cycles* 26, GB2030.
- 592 Giblin, A., Tobias, C., Song, B., Weston, N., Banta, G., Rivera-Monroy, V., 2013. The importance of  
593 dissimilatory nitrate reduction to ammonium (DNRA) in the nitrogen cycle of coastal  
594 ecosystems. *Oceanography* 26, 124-131.
- 595 Grasby, S.E., Beauchamp, B., Embry, A., Sanei, H., 2012. Recurrent Early Triassic ocean anoxia.  
596 *Geology* 41, 175-178.
- 597 Grasby, S.E., Beauchamp, B., Knies, J., 2016. Early Triassic productivity crises delayed recovery from  
598 world's worst mass extinction. *Geology* 44, 779-782.

- 599 Grice, K., Cao, C., Love, G.D., Böttcher, M.E., Twitchett, R.J., Grosjean, E., Summons, R.E., Turgeon, S.C.,  
600 Dunning, W., Jin, Y., 2005. Photic zone euxinia during the Permian-Triassic superanoxic  
601 event. *Science* 307, 706-709.
- 602 Guerrero, M.A., Jones, R.D., 1996. Photoinhibition of marine nitrifying bacteria. I. Wavelength-  
603 dependent response. *Marine Ecology Progress Series* 141, 183-192.
- 604 Hotinski, R.M., Bice, K.L., Kump, L.R., Najjar, R.G., Arthur, M.A., 2001. Ocean stagnation and end-  
605 Permian anoxia. *Geology* 29, 7-10.
- 606 Hounslow, M.W., Hu, M., Mørk, A., Weitschat, W., Vigran, J.O., Karloukovski, V., Orchard, M.J., 2008.  
607 Intercalibration of Boreal and Tethyan time scales: the magnetobiostratigraphy of the  
608 Middle Triassic and the latest Early Triassic from Spitsbergen, Arctic Norway. *Polar*  
609 *Research* 27, 469-490.
- 610 Hulth, S., Aller, R.C., Gilbert, F., 1999. Coupled anoxic nitrification/manganese reduction in marine  
611 sediments. *Geochim. Cosmochim. Acta* 63, 49-66.
- 612 Ip, Y.K., Chew, S.F., Randall, D.J., 2001. Ammonia toxicity, tolerance, and excretion. *Fish Physiology*  
613 20, 109-148.
- 614 Jenkyns, H.C., Gröcke, D.R., Hesselbo, S.P., 2001. Nitrogen isotope evidence for water mass  
615 denitrification during the Early Toarcian (Jurassic) oceanic anoxic event.  
616 *Paleoceanography* 16, 593-603.
- 617 Jensen, M.M., Lam, P., Revsbech, N.P., Nagel, B., Gaye, B., Jetten, M.S.M., Kuypers, M.M.M., 2011.  
618 Intensive nitrogen loss over the Omani Shelf due to anammox coupled with dissimilatory  
619 nitrite reduction to ammonium. *The Isme Journal* 5, 1660.
- 620 Jia, C., Huang, J., Kershaw, S., Luo, G., Farabegoli, E., Perri, M.C., Chen, L., Bai, X., Xie, S., 2012.  
621 Microbial response to limited nutrients in shallow water immediately after the end-  
622 Permian mass extinction. *Geobiology* 10, 60-71.
- 623 Junium, C.K., Arthur, M.A., 2007. Nitrogen cycling during the Cretaceous, Cenomanian-Turonian  
624 Oceanic Anoxic Event II. *Geochemistry Geophysics Geosystems* 8, Q03002.
- 625 Kidder, D.L., Worsley, T.R., 2010. Phanerozoic Large Igneous Provinces (LIPs), HEATT (Haline  
626 Euxinic Acidic Thermal Transgression) episodes, and mass extinctions. *Palaeogeogr.*  
627 *Palaeoclimatol. Palaeoecol.* 295, 162-191.
- 628 Knies, J., Grasby, S.E., Beauchamp, B., Schubert, C.J., 2013. Water mass denitrification during the  
629 latest Permian extinction in the Sverdrup Basin, Arctic Canada. *Geology* 41, 167-170.
- 630 Knoph, M.B., Thorud, K., 1996. Toxicity of ammonia to Atlantic salmon (*Salmo salar* L.) in  
631 seawater—Effects on plasma osmolality, ion, ammonia, urea and glucose levels and  
632 hematologic parameters. *Comparative Biochemistry and Physiology Part A: Physiology*  
633 113, 375-381.
- 634 Konovalov, S.K., Murray, J.W., Luther III, G.W., 2005. Basic processes of Black Sea biogeochemistry.  
635 *Oceanology* 18, 24-35.
- 636 Kump, L.R., Pavlov, A., Arthur, M.A., 2005. Massive release of hydrogen sulfide to the surface ocean  
637 and atmosphere during intervals of oceanic anoxia. *Geology* 33, 397-400.
- 638 Kuypers, M.M.M., Sliemers, A.O., Lavik, G., Schmid, M., Jørgensen, B.B., Kuenen, J.G., Sinninghe  
639 Damsté, J.S., Strous, M., Jetten, M.S.M., 2003. Anaerobic ammonium oxidation by anammox  
640 bacteria in the Black Sea. *Nature* 422, 608.

- 641 Lam, P., Jensen, M.M., Lavik, G., McGinnis, D.F., Müller, B., Schubert, C.J., Amann, R., Thamdrup, B.,  
642 Kuypers, M.M.M., 2007. Linking crenarchaeal and bacterial nitrification to anammox in the  
643 Black Sea. *Proceedings of the National Academy of Sciences* 104, 7104-7109.
- 644 Lee, P.G., 1995. Nutrition of cephalopods: Fueling the system. *Marine and Freshwater Behaviour*  
645 *and Physiology* 25, 35-51.
- 646 Lehrmann, D.J., Payne, J.L., Felix, S.V., Dillett, P.M., Wang, H., Yu, Y.Y., Wei, J.Y., 2003. Permian-  
647 Triassic Boundary Sections from Shallow-Marine Carbonate Platforms of the Nanpanjiang  
648 Basin, South China: Implications for Oceanic Conditions Associated with the End-Permian  
649 Extinction and Its Aftermath. *Palaios* 18, 138-152.
- 650 Looy, C.V., Brugman, W.A., Dilcher, D.L., Visscher, H., 1999. The delayed resurgence of equatorial  
651 forests after the Permian-Triassic ecologic crisis. *Proc. Natl. Acad. Sci. U.S.A.* 96, 13857-  
652 13862.
- 653 Luo, G.M., Wang, Y.B., Algeo, T.J., Kump, L.R., Bai, X., Yang, H., Yao, L., Xie, S.C., 2011. Enhanced  
654 nitrogen fixation in the immediate aftermath of the latest Permian marine mass extinction.  
655 *Geology* 39, 647-650.
- 656 McCready, R.G.L., Gould, W.D., Barendregt, R.W., 1983. Nitrogen isotope fractionation during the  
657 reduction of  $\text{NO}_3^-$  to  $\text{NH}_4^+$  by *Desulfovibrio* sp. *Canadian Journal of Microbiology* 29, 231-  
658 234.
- 659 Meyer, K.M., Kump, L.R., Ridgwell, A., 2008. Biogeochemical controls on photic-zone euxinia during  
660 the end-Permian mass extinction. *Geology* 36, 747-750.
- 661 Mørk, A., Elvebakk, G., Forsberg, A.W., Hounslow, M.W., Nakrem, h.A., Vigran, J.O., Weitschat, W.,  
662 1999. The type section of the Vikinghøgda Formation: a new Lower Triassic unit in central  
663 and eastern Spitsbergen. *Polar Research* 18, 51-82.
- 664 Payne, J.L., Lehrmann, D.J., Wei, J.Y., Orchard, M.J., Schrag, D.P., Knoll, A.H., 2004. Large perturbations  
665 of the carbon cycle during recovery from the End-Permian extinction. *Science* 305, 506-  
666 509.
- 667 Penn, J.L., Deutsch, C., Payne, J.L., Sperling, E.A., 2018. Temperature-dependent hypoxia explains  
668 biogeography and severity of end-Permian marine mass extinction. *Science* 362, eaat1327.
- 669 Pruss, S.B., Bottjer, D.J., Corsetti, F.A., Baud, A., 2006. A global marine sedimentary response to the  
670 end-Permian mass extinction: Examples from southern Turkey and the western United  
671 States. *Earth-Sci. Rev.* 78, 193-206.
- 672 Quan, T.M., Falkowski, P.G., 2009. Redox control of N:P ratios in aquatic ecosystems. *Geobiology* 7,  
673 124-139.
- 674 Rabalais, N.N., Turner, R.E., Wiseman, W.J., 2002. Gulf of Mexico Hypoxia, a.k.a. "The Dead Zone".  
675 *Annual Review of Ecology and Systematics* 33, 235-263.
- 676 Schobben, M., Stebbins, A., Ghaderi, A., Strauss, H., Korn, D., Korte, C., 2015. Flourishing ocean drives  
677 the end-Permian marine mass extinction. *Proceedings of the National Academy of Sciences*  
678 112, 10298-10303.
- 679 Schobben, M., Stebbins, A., Ghaderi, A., Strauss, H., Korn, D., Korte, C., 2016. Eutrophication,  
680 microbial-sulfate reduction and mass extinctions. *Communicative & Integrative Biology* 9,  
681 e1115162.

- 682 Schoepfer, S.D., Henderson, C.M., Garrison, G.H., Ward, P.D., 2012. Cessation of a productive coastal  
683 upwelling system in the Panthalassic Ocean at the Permian–Triassic Boundary.  
684 *Palaeogeogr. Palaeoclimatol. Palaeoecol.* 313-314, 181-188.
- 685 Scotese, C.R., Moore, T.L., 2014. Atlas of Phanerozoic Ocean Currents and Salinity (Mollweide  
686 Projection), PALEOMAP Project PaleoAtlas for ArcGIS, PALEOMAP Project, Evanston,  
687 Illinois.
- 688 Sigman, D., Karsh, K., Casciotti, K., 2009. Ocean process tracers: nitrogen isotopes in the ocean,  
689 *Encyclopedia of Ocean Science*, 2nd edition. Elsevier, Amsterdam, pp. 4138-4153.
- 690 Smith, J.M., Chavez, F.P., Francis, C.A., 2014. Ammonium Uptake by Phytoplankton Regulates  
691 Nitrification in the Sunlit Ocean. *PLoS ONE* 9, e108173.
- 692 Song, H., Tong, J., Algeo, T.J., Song, H., Qiu, H., Zhu, Y., Tian, L., Bates, S., Lyons, T.W., Luo, G., Kump,  
693 L.R., 2014. Early Triassic seawater sulfate drawdown. *Geochim. Cosmochim. Acta* 128, 95-  
694 113.
- 695 Stüeken, E.E., Kipp, M.A., Koehler, M.C., Buick, R., 2016. The evolution of Earth's biogeochemical  
696 nitrogen cycle. *Earth-Sci. Rev.* 160, 220-239.
- 697 Sun, Y.D., Joachimski, M.M., Wignall, P.B., Yan, C.B., Chen, Y.L., Jiang, H.S., Wang, L.N., Lai, X.L., 2012.  
698 Lethally hot temperatures during the Early Triassic greenhouse. *Science* 338, 366-370.
- 699 Sun, Y.D., Wignall, P.B., Joachimski, M.M., Bond, D.P.G., Grasby, S.E., Sun, S., Yan, C.B., Wang, L.N.,  
700 Chen, Y.L., Lai, X.L., 2015. High amplitude redox changes in the late Early Triassic of South  
701 China and the Smithian/Spathian extinction. *Palaeogeogr. Palaeoclimatol. Palaeoecol.* 427,  
702 62-78.
- 703 Toseland, A., Daines, S.J., Clark, J.R., Kirkham, A., Strauss, J., Uhlig, C., Lenton, T.M., Valentin, K.,  
704 Pearson, G.A., Moulton, V., Mock, T., 2013. The impact of temperature on marine  
705 phytoplankton resource allocation and metabolism. *Nature Climate Change* 3, 979-984.
- 706 Twitchett, R.J., 2007. The Lilliput effect in the aftermath of the end-Permian extinction event.  
707 *Palaeogeogr. Palaeoclimatol. Palaeoecol.* 252, 132-144.
- 708 U.S. Environmental Protection Agency, 1998. Addendum to "Ambient Water Quality Criteria for  
709 Ammonia--1984.", in: Service, N.T.I. (Ed.), Springfield, VA.
- 710 Van Cappellen, P., Ingall, E.D., 1994. Benthic phosphorus regeneration, net primary production, and  
711 ocean anoxia: A model of the coupled marine biogeochemical cycles of carbon and  
712 phosphorus. *Paleoceanography* 9, 677-692.
- 713 Van Mooy, B.A.S., Keil, R.G., Devol, A.H., 2002. Impact of suboxia on sinking particulate organic  
714 carbon: Enhanced carbon flux and preferential degradation of amino acids via  
715 denitrification. *Geochim. Cosmochim. Acta* 66, 457-465.
- 716 Voight, J.R., Pörtner, H.O., O'Dor, R.K., 1995. A review of ammonia-mediated buoyancy in squids  
717 (cephalopoda: Teuthoidea). *Marine and Freshwater Behaviour and Physiology* 25, 193-  
718 203.
- 719 Wignall, P.B., Bond, D.P.G., Sun, Y., Grasby, S.E., Beauchamp, B., Joachimski, M.M., Blomeier, D.P.G.,  
720 2016. Ultra-shallow-marine anoxia in an Early Triassic shallow-marine clastic ramp  
721 (Spitsbergen) and the suppression of benthic radiation. *Geol. Mag.* 153, 316-331.
- 722 Wignall, P.B., Twitchett, R.J., 2002. Extent, duration, and nature of the Permian-Triassic superanoxic  
723 event. *Geol. Soc. Am. Spec. Paper* 356, 395-413.

724 Winguth, A.M.E., Shields, C.A., Winguth, C., 2015. Transition into a Hothouse World at the Permian–  
725 Triassic boundary—A model study. *Palaeogeogr. Palaeoclimatol. Palaeoecol.* 440, 316-327.

726 Xie, S., Pancost, R.D., Wang, Y., Yang, H., Wignall, P.B., Luo, G., Jia, C., Chen, L., 2010. Cyanobacterial  
727 blooms tied to volcanism during the 5 m.y. Permo-Triassic biotic crisis. *Geology* 38, 447-  
728 450.

729 Zehr, J.P., Ward, B.B., 2002. Nitrogen cycling in the ocean: new perspectives on processes and  
730 paradigms. *Applied and Environmental Microbiology* 68, 1015-1024.

731 Zhang, X., Sigman, D.M., Morel, F.M.M., Kraepiel, A.M.L., 2014. Nitrogen isotope fractionation by  
732 alternative nitrogenases and past ocean anoxia. *Proc. Natl. Acad. Sci. U.S.A.* 111, 4782-  
733 4787.

734 Zhao, L., Chen, Y., Chen, Z.-q., Cao, L., 2013. Uppermost Permian to Lower Triassic Conodont  
735 Zonation from Three Gorges Area, South China. *Palaios* 28, 523-540.  
736

737 **Figure and table captions**

738 Fig. 1 The marine nitrogen cycle with sub-models for oxic (A), anoxic (B) and euxinic (C)  
739 conditions. Blue arrows are aerobic reactions; red arrows are anaerobic reactions;  
740 black arrows are reactions with aerobic and anaerobic pathways. Bold lines are  
741 favoured reactions, whereas dashed lines are possible, but unfavoured reactions.  
742 Lightning contributes ~5-8 % of total fixed nitrogen and is generally considered as a  
743 constant input in geological studies. Sub-models represent end-member situations  
744 and do not include the oxygen minimum zone in oxic oceans and oxygenated surface  
745 layers in anoxic and euxinic oceans. In model B, nitrate is consumed by reactions 5, 6,  
746 7 and 8 while resupply of nitrate is inhibited because reaction 4 is a light-inhibited  
747 aerobic reaction. In the model C, nitrogen fixation can be inhibited due to removal of  
748 metabolizable Mo, V and Fe in the water column, leading to suppression of the  
749 nitrogen cycle. Nutrient-N systematically becomes dominated by  $\text{NH}_3/\text{NH}_4^+$  in anoxic  
750 and euxinic conditions. Anammox = anaerobic ammonium oxidation, DNRA =  
751 dissimilatory nitrate reduction to ammonium.

752 Fig. 2 A., Early Triassic palaeogeography, ocean currents and sites of microbial buildups  
753 (Pruss et al., 2006; Chen et al., 2014; Scotese and Moore, 2014). B., Temporal  
754 occurrences of microbial buildups (geographic occurrences shown in A), redox  
755 conditions and equatorial seawater temperatures (Wignall and Twitchett, 2002;  
756 Grasby et al., 2012; Sun et al., 2012; Sun et al., 2015) in the Early Triassic. For redox  
757 conditions, the blue colour stands for a globally oxic condition; black stands for  
758 generally anoxic condition while white stands for regional oxic conditions in some  
759 basins. [These redox histories derive from studies in Alps, British Columbia, Canadian  
760 Arctic, Japan, South China, Spitsbergen etc.](#) C., Simplified models comparing nitrogen  
761 cycles between a well oxygenated nitrate ocean and an Early Triassic stratified  
762 ammonium ocean. Note that in anoxic oceans denitrification can occur in all water  
763 depths while nutrient-N uptake by phytoplankton can only occur in the euphotic zone.

764 Fig. 3 Cross plots of total nitrogen and total organic carbon content of decarbonatized  
765 sample residues. Intercepts on the TN axis indicate the presence of excess silicate-  
766 bound nitrogen in the samples.

767 Fig. 4 Geochemical records from three study sections, showing a gradual decrease in  $\delta^{15}\text{N}$   
768 in the Early Triassic, a negative shift in  $\delta^{15}\text{N}$  towards the S-S boundary, the covariation  
769 of  $\delta^{13}\text{C}_{\text{carb}}$  and  $\delta^{13}\text{C}_{\text{org}}$  at Jiarong and a near antithetic relationship between  $\delta^{15}\text{N}$  and  
770  $\text{C}/\text{N}_{\text{atomic}}$ . Redox conditions and biostratigraphy from the three sections,  $\delta^{13}\text{C}_{\text{carb}}$  from  
771 Jiarong and  $\delta^{13}\text{C}_{\text{org}}$  from Vindodden are from Zhao et al., (2013), Sun et al. (2015),  
772 Wignall et al. (2016) and Elrick et al. (2017). Redfield ratio ( $\text{C}/\text{N}=6.6$ ) is used as a  
773 reference.

774 Fig. 5 Summary of published  $\delta^{15}\text{N}$  records in the Late Permian to Early Triassic interval,  
775 showing strong denitrification occurred geographically in different settings across the  
776 P-T boundary. The onset and duration of the P-T water column denitrification shows  
777 regional variations, probably controlled by local redox conditions and  
778 palaeoceanographic settings.

779 Fig. 6 Cross plots of V vs. Al, Mo vs. Al, Fe vs. Al and P vs. Al from Jiarong, South China. The  
780 original dataset is fully accessible in Sun et al. (2015).

781 Fig. 7 Depth profile of  $\text{NO}_3^-$ ,  $\text{NH}_4^+$ ,  $\text{O}_2$  and  $\text{S}^{2-}$  concentrations in the highly stratified  
782 contemporary Black Sea, showing a depletion of  $\text{NO}_3^-$  but accumulation of  $\text{NH}_4^+$  in  
783 anoxic water column (modified from Konovalov et al., 2005).

784 Fig. 8 The evolution of the ammonium ocean and changes in energy structures in the  
785 aftermath of the end-Permian mass extinction.

786 Table 1 Comparison of energy yields (standard Gibbs free energy) of aerobic and anaerobic  
787 respiration. Glucose ( $\text{C}_6\text{H}_{12}\text{O}_6$ ) is the most important source of energy for cellular  
788 respiration and thus is used for calculation of comparable energy yields here. Isotopic  
789 enrichment ( $\epsilon$ ) is only for nitrogen reactions and approximated by  $\delta^{15}\text{N}_{\text{product}} -$   
790  $\delta^{15}\text{N}_{\text{reactant}}$  (for  $\epsilon < 1000$  ‰) (McCready et al., 1983; Sigman et al., 2009; Zhang et al.,  
791 2014). Note that DNRA produces less energy than denitrification in term of per mol C;  
792 however, in intense anoxia where nitrate is a limited resource, DNRA yields more  
793 energy than denitrification in measure of per mole N.

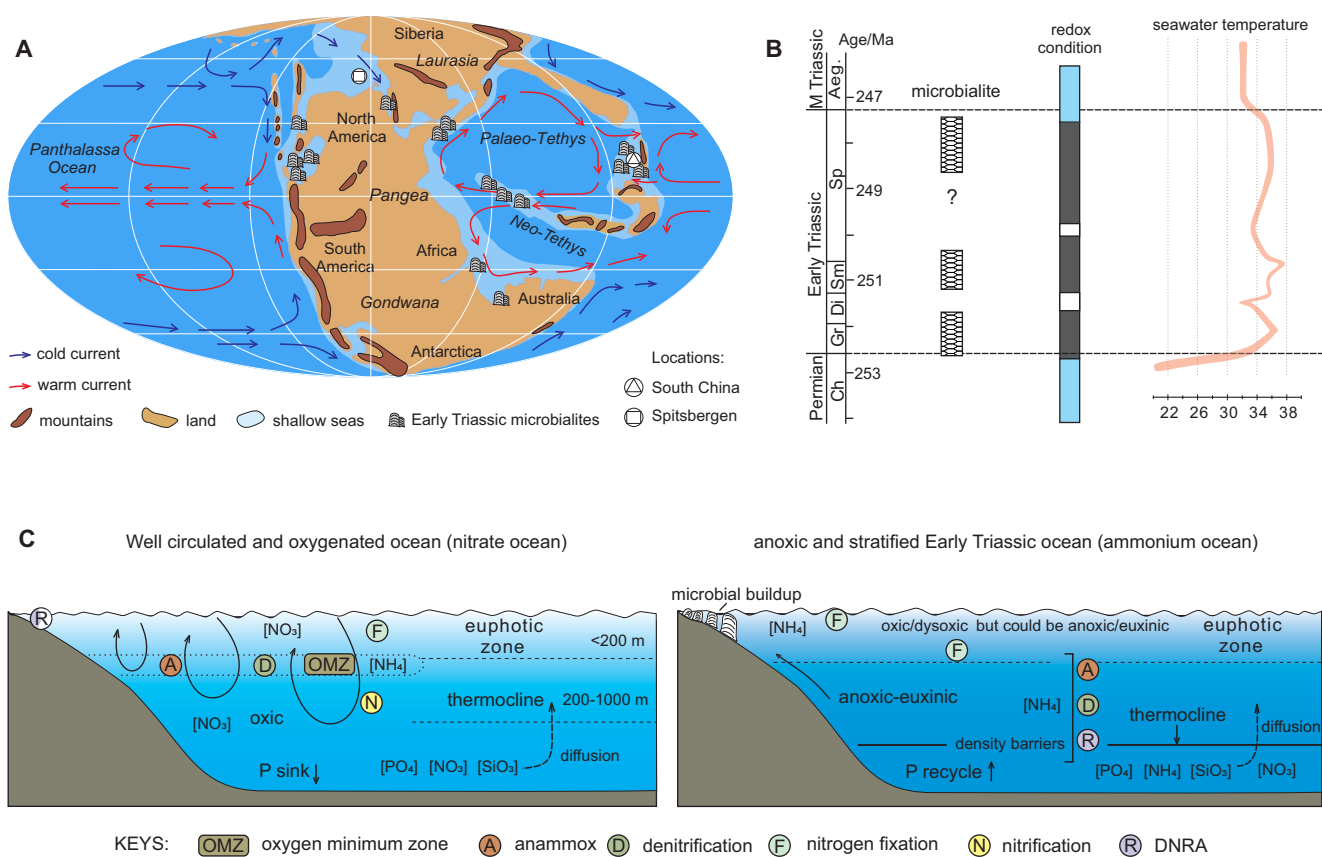
794 Table 2 A comparison of  $\delta^{15}\text{N}$  and  $\text{C}/\text{N}_{\text{atomic}}$  ratio in clay-poor rocks and clay-rich rocks that  
795 are closely spaced to each other, showing measured  $\delta^{15}\text{N}$  and  $\text{C}/\text{N}_{\text{atomic}}$  ratios are

796 generally consistent in the two types of rock but  $C/N_{\text{atomic}}$  ratios are more variable in  
797 Early Triassic (TOC poor) rocks.

798 Supplementary materials: Data file (including the original dataset and statistical analyses  
799 on the data)

800



**Figure 2**[Click here to download Figure: Fig. 2 maps and ocean models.pdf](#)

**Figure 3**

[Click here to download Figure: Fig. 3 TN-TOC cross plot.pdf](#)

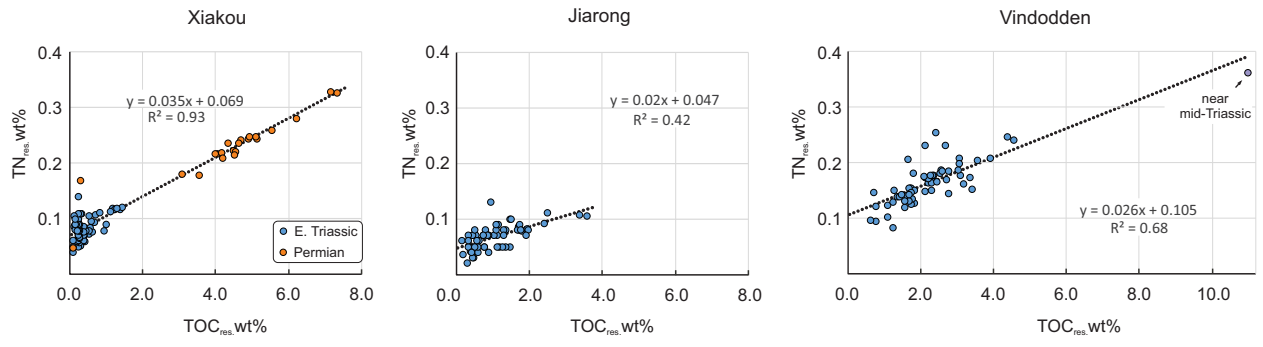


Figure 4

[Click here to download Figure: Fig. 4 Logs.pdf](#)

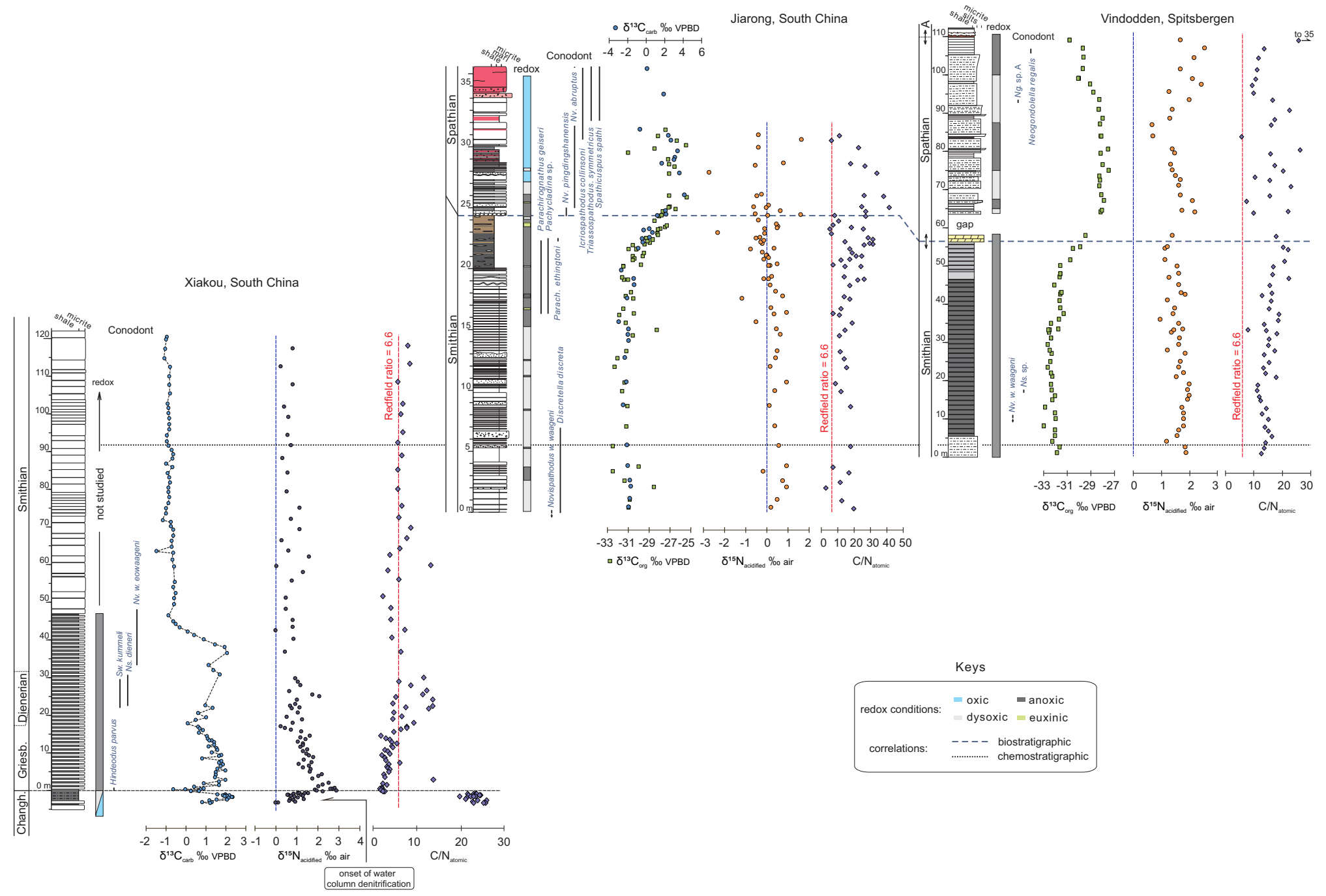




Figure 6

[Click here to download Figure: Fig. 6 trace metal cross plot.pdf](#)

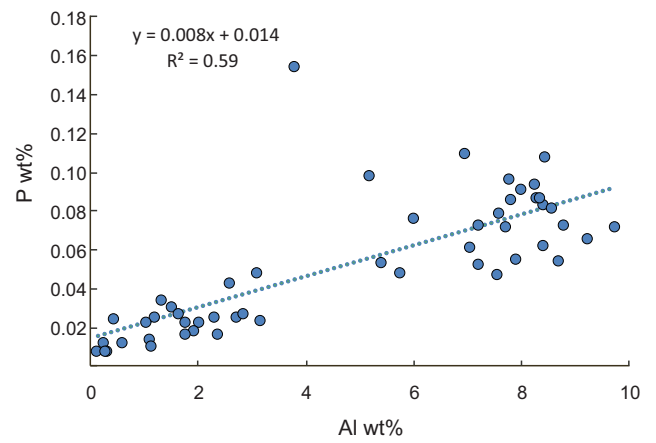
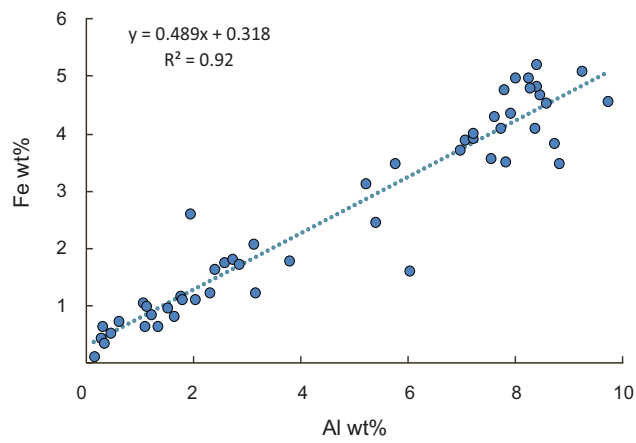
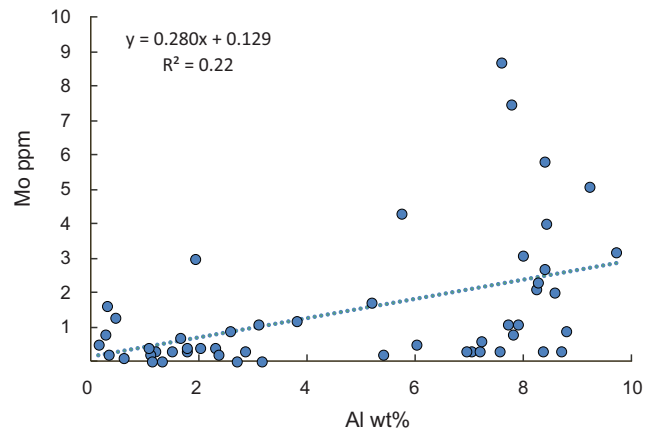
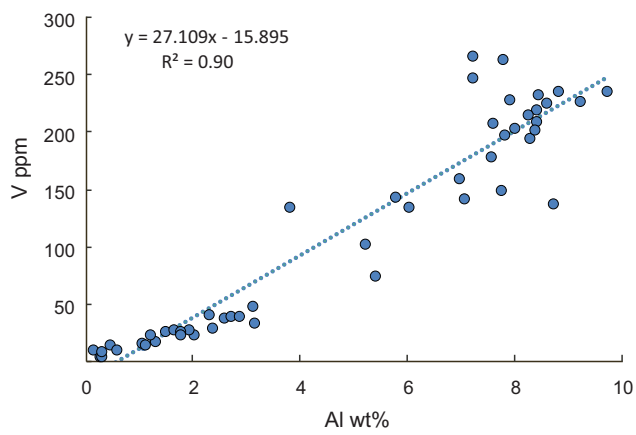


Figure 7  
[Click here to download Figure: Fig. 7 Black sea.pdf](#)

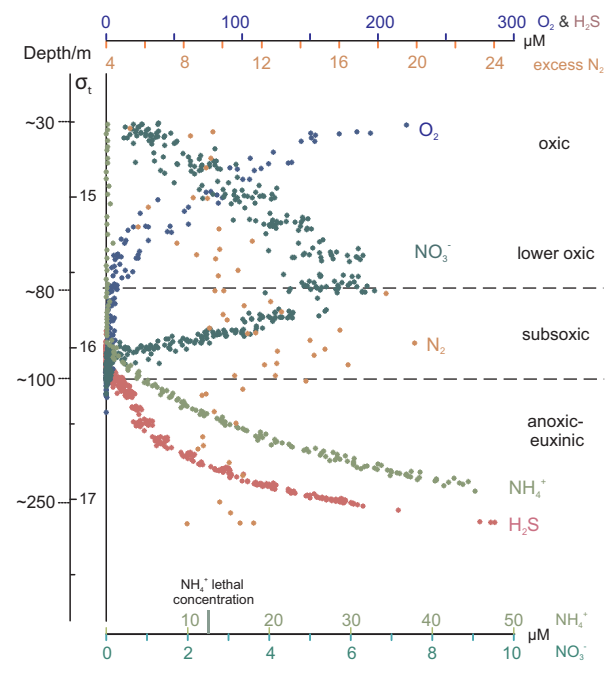
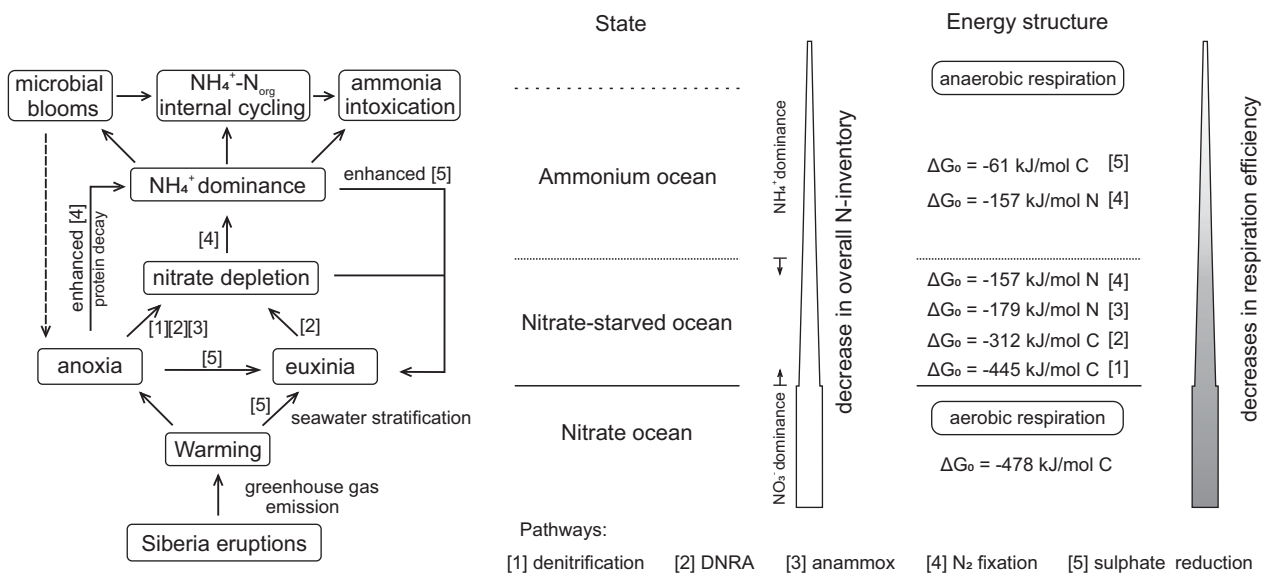


Figure 8

[Click here to download Figure: Fig. 8 flow chart.pdf](#)



**Table 1**[Click here to download Table: Table 1 formal.pdf](#)

Energy pathway	Simplified reaction	Energy yield ( $\Delta G^0$ )			isotope effect ( $\epsilon$ )
		kJ/mol C	kJ/mol N	kJ/mol S	‰
aerobic respiration	$C_6H_{12}O_6 + 6O_2 = 6CO_2 + 6H_2O$	-478	--	--	
denitrification	$5C_6H_{12}O_6 + 24NO_3^- + 24H^+ = 30CO_2 + 12N_2 + 42H_2O$	-445	-556	--	5-30
DNRA	$C_6H_{12}O_6 + 3NO_3^- + 6H^+ = 6CO_2 + 3NH_4^+ + 3H_2O$	-312	-623	--	unknown
anammox	$NH_4^+ + NO_2^- = N_2 + 2H_2O$	--	-179	--	>10
nitrogen fixation	$N_2 + 10H^+ + 8e^- = 2NH_4^+ + H_2$	--	-157	--	-1 to 2 <sup>a</sup> or to -7 <sup>b</sup>
sulphate reduction	$C_6H_{12}O_6 + 3SO_4^{2-} = 6CO_2 + 6H_2O + 3S^{2-}$	-61	--	-121	
ethanol fermentation	$C_6H_{12}O_6 = 2CO_2 + 2C_2H_5OH$	-38	--	--	

a., reaction catalyzed by Mo-Fe nitrogenase enzyme;

b., reaction catalyzed by V-Fe or Fe-only nitrogenase enzyme.

**Table 2**[Click here to download Table: Table 2.pdf](#)

Sample No.	Height/m	Lithology	carbonate content/%	TOC/ wt%	TN/ wt%	$\delta^{13}\text{C}_{\text{org}}$ ‰	$\delta^{15}\text{N}$ ‰	C/N <sub>atomic</sub>
<b>Permian (high TOC) samples</b>								
XK 248B	-0.88	limestone	74.7	1.13	0.06	-26.13	1.05	23.5
XK 248A	-0.81	marl	14.4	3.05	0.15	-26.35	1.36	23.1
XK 247A	-0.90	limestone	73.2	1.21	0.06	-26.11	1.53	23.8
XK 247B	-0.95	marl	29.3	2.86	0.15	-26.13	1.10	21.8
<b>Triassic (low TOC) samples</b>								
XK 22.1	22.1	limestone	92.5	0.03	0.01	-28.74	1.13	7.5
XK 21.9	21.9	black shale	19.3	1.05	0.10	-28.57	0.76	12.7

dataset and additional statistical analyses

[Click here to download Supplementary material for online publication only: Supplementary material \[final\].pdf](#)